NASA
Technical
Paper
2095

January 1983

Vibration Studies of a Lightweight Three-Side Membrane Suitable for Space Application

John L. Sewall,
Robert Miserentino,
and Richard S. Pappa

NASA

NASA
Technical
Paper
2095

1983

Vibration Studies of a Lightweight Three-Sided Membrane Suitable for Space Application

John L. Sewall,
Robert Miserentino,
and Richard S. Pappa
Langley Research Center
Hampton, Virginia

National Aeronautics
and Space Administration

**Scientific and Technical
Information Branch**

Identification of commercial products in this report is used to adequately describe the model. The identification of these commercial products does not constitute official endorsement, expressed or implied, of such products or manufacturers by the National Aeronautics and Space Administration.

SUMMARY

Vibration studies carried out in a vacuum chamber are reported for a three-sided membrane that is a candidate for reflective surfaces in space antennas. The membrane was a single sheet of aluminized Mylar[1] with inwardly curved edges. Uniform tension was transmitted by thin steel cables encased in the edges. A moderate range of tension loads, less than 262 N (59 lb), was applied to the cables at each apex. Variation of ambient air pressure from atmospheric to near vacuum resulted in increased response frequencies and amplitudes. The membrane was found to be lowly damped, less than 1.4 percent, regardless of the air pressure. The first few vibration modes measured in a near vacuum are shown to be predictable by a finite-element structural analysis over a range of applied tension loads. For a given mode the square of the frequency varied in a linear manner with tension. This result may be useful, through simple relations, for estimating frequencies and tension loads of other dynamically similar membranes. The complicated vibration mode behavior observed during tests at various air pressures is studied analytically with a nonstructural effective air-mass approximation.

INTRODUCTION

Current concepts for large space structures include requirements for reflecting surfaces for antennas and collectors. A type of structure under evaluation consists of flat pretensioned membrane facets oriented in contiguous segments to approximate spherical or paraboloidal surfaces. Also, large pretensioned membranes may be used in phased arrays. Collectors with three- and six-sided facets tensioned by cables between joints on the surface of a large truss are described in reference 1. High efficiency and stability of the collector require some form of dynamic controls, which in turn depend on an adequate understanding of vibration characteristics, not only of the overall collectors but also of the individual membrane facets. This paper is concerned with vibrations of the facets.

Analytical studies of the vibration of membranes with an arbitrary number of sides (or edges) are the subject of references 2 to 7. Reference 2 compares the vibration modes of regular polygonal membranes ranging from triangular to decagonal. A more detailed classification of vibration modes for triangular and hexagonal membranes is given in reference 3 in an application of symmetry concepts and group theory. The other analytical studies feature conformal transformations of polygons to circles (refs. 4 and 5), curved edges as well as straight edges (ref. 6), and interior point supports (ref. 7). A related vibration study of a simply supported triangular plate (ref. 8) offers the rare presentation of both experimental and analytical vibration modes under one cover.[2] The supported-edge boundary condition is significantly different from the discrete connections generally needed for a membrane facet. None of the references considered the possible effects of the surrounding medium (i.e., ambient air or vacuum). These effects can be negligible, as

---

[1]Mylar: trademark of E. I. duPont de Nemours & Co., Inc.

[2]A classified experimental and analytical investigation of membrane vibrations, including effects of vacuum and ambient air pressure, has recently been carried out by George Jacobson and associates, of the Grumman Aerospace Corporation.

in reference 8 for a relatively heavy membrane or plate, but merit consideration for a lightweight panel, such as a collector facet.

The purpose of the present paper is to report an experimental and analytical study undertaken to determine the basic vibration behavior of a thin equilateral triangular-shaped membrane tensioned by thin cables along the edges and discretely fixed at short cable extensions beyond the apexes. The membrane was mounted in a vacuum chamber and vibration-tested over a moderate range of tension levels at ambient air pressures from atmospheric to near vacuum. Experimental out-of-plane vibration modes (i.e., frequencies, mode shapes, and damping coefficients) are correlated with frequencies and mode shapes calculated with the SPAR finite-element structural analysis computer program (ref. 9).

To realistically simulate the reflective function of the facet, the membrane was made of aluminized Mylar with the cables encased along inwardly curved edges and joined at the apexes. This design is intended to produce uniform internal membrane tension sufficient to achieve optical-quality flatness, in accordance with the requirements specified in reference 10.

Results of this study are presented to show chiefly the effects of tension and ambient air pressure (or density) on resonant (or natural) frequencies of vibration and corresponding mode shapes. The effect of air pressure on damping is also included. Variations of frequency parameters with tension form the basis for establishing scale factors, as shown in appendix A, for estimating frequencies and tensions for other dynamically similar membranes. Appendix B shows how analytical frequencies of the membrane are affected by an approximation of the virtual mass of air at various pressures.

SYMBOLS

A cross-sectional area of cable

d cable diameter

E Young's modulus of elasticity

f frequency, Hz

g structural damping coefficient, $\frac{2 \times \text{Viscous damping coefficient}}{\text{Critical damping coefficient}}$

L reference (or representative) length

m_i air mass per unit area on ith membrane element (appendix B)

N_n tension per unit length, normal to the membrane edge, $T/2R$

R radius of membrane edge

r_i radius of arc in plane of ith membrane element centroid (fig. 18)

T tension load at membrane apex

t	membrane thickness
$w(x,y)$	normalized amplitude of response of membrane
x,y	Cartesian coordinates
z_i	assumed height of ambient air mass above ith membrane centroid (appendix B)
α	coefficient of thermal expansion
δ	boundary displacements (fig. 8)
ε	in-plane strain
λ	geometric scale factor (appendix A)
μ	Poisson's ratio
ξ_i	coordinate of ith membrane element centroid in ξz-plane (fig. 18)
ρ	mass density
ρ_a	mass density of surrounding air (fig. 18)
σ	stress
ω	angular frequency, $2\pi f$, rad/sec

Subscripts:

c	cable
i	membrane finite element (appendix B)
M	model of present investigation (appendix A)
m	membrane
P	another model, or prototype (appendix A)
r	approximate air mass at partial atmosphere, less than 1 atm (1 atm = 101.325 kPa)
1	approximate air mass at reference atmosphere, 760 mm Hg (1 mm Hg = 133.322 Pa)

Abbreviations:

FFT	fast Fourier transform
ITD	Ibrahim time domain
TF	transfer function

VIBRATION TEST PROGRAM

The test portion of the study was conducted in the Structural Dynamics Research Laboratory at the Langley Research Center. Out-of-plane vibration modes (i.e., frequencies, mode shapes, and damping coefficients) were measured from responses excited by low sinusoidal and random input forces. The use of both these test approaches enhanced mode identification and improved the confidence in the reported modal data. The principal modal data were obtained to determine the effects of vibrations in membrane tension and air pressure.

Membrane Test Specimen

Basic geometrical features of the equilateral three-sided membrane are given in figure 1. The membrane was made from 0.0127-mm (0.0005-in.) thick Mylar with a vapor-deposited aluminum coat. Each edge of the membrane was a circular arc of radius 1.41 m (55.5 in.) with a 19.05-mm (0.75-in.) Mylar hem through which passed a 1.60-mm (0.063-in.) diameter steel cable. As indicated in the detail in the figure, the hem was bonded to both sides of the membrane. The maximum hem thickness was 0.038 mm (0.0015 in.). The chord length of each side was 0.914 m (36 in.). Structural properties of the model are given in table I. At each of the three apexes, the pair of edge cables was joined to form a single cable which continued over pulleys to the opposite side of the membrane and was attached to the center ring, as illustrated in figure 2.

Test Apparatus

The membrane was secured, as shown in figure 3, within a stiff steel frame mounted inside an 8-foot-diameter spherical vacuum chamber at the Langley Research Center. The smooth reflective quality of the aluminized Mylar surface is evident, and wrinkles were confined to regions near the apexes. The smooth surface was maintained at optical-quality flatness by tension loads that gave membrane stresses above 0.05 times the membrane yield stress. When the model was initially mounted and tensioned to that level, the edges were manually moved along the cables to obtain a smooth distribution of the membrane along the circular arcs. This adjustment helped to satisfy the requirement specified in reference 10 for uniform tension in the membrane.

The accelerometers shown in figure 3 were used to monitor vibration responses of various parts of the mounting frame and the center ring. Outputs from these accelerometers showed that responses during vibration tests were insignificant compared with responses of the membrane. Thus, the frame was assumed to be rigid.

Modal survey rig.- Also shown in figure 3 are a deflectometer and track comprising an automated, remotely controlled apparatus for obtaining dynamic responses over a wide portion of the membrane surface. The deflectometer is a noncontacting capacitance-type device which is sensitive to minute movements of the membrane within a small gap at the end of the probe. Automatic maintenance of a constant mean gap while moving the probe to various structural locations is crucial to the reliability of the measurement. The capacitance-type proximity deflectometer was chosen because the output is unaffected by low pressure or membrane thickness. The performance of inductance-type deflectometers suffered at near-vacuum pressures, primarily because this lightweight material is sensed with the assistance of eddy currents induced in

the air ordinarily in the gap and because of outgassing. This problem is identified in reference 11 for consideration in the design of any electrical instrument for space applications.

The deflectometer was mounted as shown in figure 3 for movement by remote control in three orthogonal directions. Dynamic responses were measured, as shown in figure 4, over the main part of the surface, away from the wrinkled apex regions where local amplitude distortions occurred. The shapes of sinusoidally excited modes were automatically plotted as a family of curves showing peak amplitudes for each horizontal traverse of the deflectometer, and the shapes of randomly excited modes were obtained from amplitude measurements at 130 discrete points.

Electrodynamic shaker.- Membrane out-of-plane vibration modes were excited by an electrodynamic shaker attached to the cable leading from the lowest apex, as shown in figures 2 and 3. The shaker attachment consisted of a thin rod which passed through a ring in the shaker-support cable and a force gage which monitored the input dynamic force. The effective mass of the shaker moving with the model (half the force gage and all its attachments to the cable) was 19.7 grams. The shaker can generate up to 4.4 N of force; however, no more than 0.001 of this was needed to excite the membrane vibration modes to acceptable levels for the vibration instrumentation.

Membrane tension.- In-plane tension of the membrane was maintained by the steel cables passing over the pulleys and continuing to the back-surface support structure. Variation and control of the tension were accomplished either manually by adjusting the turnbuckles shown in figures 2 and 3 or automatically by remote control of an electric motor and tension actuator in the apparatus of figure 5. As shown in figure 5(a), the front and backside tension cables both passed over the bottom pulley to the load cell and tension actuator. The shaker-support combination of pulleys and cables assured a horizontally oriented shaker input regardless of the magnitude of the tension. This apparatus allowed the cable tension to be readily varied and controlled at reduced air pressures over the 89 to 262 N (20 to 59 lb) tension range.

Test Procedures and Instrumentation

The test procedures are designated on the basis of the way the membrane was excited, namely, sinusoidal force input and random force input. Each approach involves three principal functions: (1) excitation and its control, (2) response measurements on the structure, and (3) data processing to obtain vibration-mode data (i.e., frequencies, mode shapes, and damping coefficients). These functions are represented for these tests in the flow charts of figure 6.

Sinusoidal input.- In the sinusoidal-input procedure, the membrane was subjected to sinusoidally varying forces at frequencies ranging from about 10 to 100 Hz. The membrane responded to this excitation at resonant frequencies that were identified and processed by separation of the coincident and quadrature components of the response. (See, e.g., the co-quad method of ref. 12.) This procedure is represented by the flow chart in figure 6(a). The distribution of out-of-plane response amplitudes over the membrane surface in the form of a mode shape was plotted with the x-y plotter for each resonant frequency over the region shown in figure 4.

Damping properties of the vibration modes were defined in the form of coefficients or percentages of critical damping by three methods based on the sinusoidal-input approach. One of these is the Kennedy-Pancu method, which is related to the co-quad method but involves transformation of responses onto the complex plane, as

in Nyquist plots. This method is described in references 13 and 14. The second method is based on magnitude and width of the resonant response amplitude on an individual amplitude-versus-frequency plot (e.g., ref. 15, p. 77). The third method is the logarithmic-decrement method, in which the damping is estimated from the history of a decaying oscillatory response following cutoff of the excitation (e.g., ref. 15, p. 72).

Random input.- In the random-input procedure, represented by the flow chart in figure 6(b), the membrane was subjected to random forces from a band-limited white noise generator at a range of frequencies between 12 and 100 Hz. Vibration modes in this range were identified by two methods of modal extraction from random dynamic data. One of these methods is called the transfer function (TF) method (ref. 16), which uses a commercial modal analyzer. The other method operates in the time domain rather than the frequency domain. This method uses the Ibrahim time domain (ITD) procedure, which is described in references 17 and 18. An essential element of both methods in this investigation was the fast Fourier transform (FFT), which is a tool for numerically computing transfer functions from digitized random data; however, FFT is not in general required for ITD. With each method, mode shapes for several vibration modes were obtained from random responses at each of the 130 points distributed over the membrane surface.

VIBRATION ANALYSIS

Analyses were conducted with the SPAR finite-element structural analysis computer program (ref. 9) for comparison with experimentally determined vibration modes obtained in a near vacuum. In using SPAR to calculate out-of-plane vibration modes, the Mylar surface was modeled by membrane elements; the steel cable was modeled by axial elements. Since neither of these finite elements can sustain bending, out-of-plane stiffness is entirely due to in-plane tension which produces the differential stiffness.

SPAR Model and Boundary Conditions

Because of equilateral geometry and overall uniformity of the membrane, symmetry was assumed about a vertical axis through the membrane centroid, the bottom apex, the cable, and the pulley. (See fig. 1.) On this basis, analytical half-models (fig. 7) were used. Thus, computed vibration modes were either symmetric or antisymmetric according to displacement and slope constraints specified along the axis of symmetry. Triangular and quadrilateral membrane elements made up the interior surface inside the hem. The hem was modeled mostly with quadrilateral membrane elements, each 3 times as thick as the interior surface elements. (See fig. 1.) Alternate finite-element models (fig. 7) were used in order to investigate convergence of the analytical solutions. The cables running through the casing of the membrane edge and extending beyond the apexes were modeled with pretensioned linear elements having no bending stiffness. The part of the shaker moving with the membrane during vibration was simulated as a rigid mass (half the measured value for the half-model) and located 38.1 mm (1.5 in.) below the bottom apex.[3]

[3]The presence of a local rigid mass precludes applying triaxial symmetry in a smaller (pie-shaped) finite-element model together with symmetric and antisymmetric boundary conditions, as was done for the equilateral triangular membrane in reference 3.

All edges of the membrane were considered free. The cables were assumed to extend beyond the apexes to points corresponding to the pulley centerlines, as indicated in figures 1 and 4. The out-of-plane and lateral in-plane displacements of the cable end points were constrained, but the axial displacements were left free.

Tension Application and Uniformity

Tension was applied equally at the cable ends in a direction aligned with the cable between its end and the apex. During this loading, the membrane was constrained in all degrees of freedom at the center grid point on the axis of symmetry, and only in-plane displacements were allowed elsewhere. The tension was assumed to be transmitted uniformly along the cable to the membrane through casings along the inwardly curved circular-arc edges.

The basic relationship governing tension along each curved edge is (based on ref. 10)

$$\frac{T}{2} = N_n R \tag{1}$$

where T is the tension applied at the cable end, R is the edge radius of curvature, and N_n is the normal load per unit length along the edge. The requirement for uniform biaxial stress throughout the membrane is

$$\sigma_x = \sigma_y = \frac{N_n}{t} \tag{2}$$

where σ_x and σ_y are in-plane stresses in the x-direction and y-direction, respectively, and t is the thickness of the membrane (interior to the hem).

The sliding of the membrane edges along the cables to satisfy this requirement in the test model implies the absence of constraint due to differences in the elastic properties of membrane and cable. This condition of relative movement between the two materials was represented analytically by defining the difference in strain between them in terms of a temperature difference $\Delta\tau$ in the cable;[4] i.e.,

$$\alpha_c \Delta\tau = \varepsilon_m - \varepsilon_c \tag{3}$$

where α_c is the coefficient of thermal expansion of the cable, ε_m is the membrane strain, and ε_c is the cable strain. From equations (1) and (2) and the following stress-strain relations

$$\varepsilon_m = \frac{(1 - \mu_m)\sigma_m}{E_m} \tag{4a}$$

[4]This method was suggested by Melvin Anderson of the NASA Langley Research Center.

$$\varepsilon_c = \frac{\sigma_c}{E_c} = \frac{T}{2AE_c} \tag{4b}$$

for both membrane and cable, equation (3) becomes

$$\Delta\tau = \frac{T}{2\alpha_c}\left(\frac{1 - \mu_m}{E_m Rt} - \frac{4}{E_c \pi d^2}\right) \tag{5}$$

where μ_m is Poisson's ratio for the membrane, E_m is the modulus of elasticity of the membrane, $A = \frac{\pi d^2}{4}$ is the cable cross-sectional area in terms of its diameter d, and E_c is the modulus of elasticity of the cable. From the values listed in table I, $\Delta\tau$ was computed for each tension T and introduced along with T as average temperature for each of the axial elements between the apexes, in accordance with the instructions of reference 9.

The uniform stress requirement of equation (2) was verified by SPAR results, and magnitudes of interior stresses are listed in figure 8 for three tension loads. Calculated boundary displacements also are included.

RESULTS AND DISCUSSION

The principal results of this study, presented in figures 9 to 17 and tables II and III, show the effects of the tension and ambient air pressure on the membrane vibration modes. Variations of tension from 89 to 262 N (20 to 59 lb) resulted in linear frequency parameter trends (fig. 13) that appear to be useful for estimating vibration modes of dynamically similar membranes. Variations of air pressure from atmospheric to near vacuum altered the sequence of vibration modes and changed resonant frequencies and response amplitudes, as shown in figure 14. The effects of air-pressure variations on damping are shown in figure 15. The ordinate air pressure in figures 14 and 15 is defined in terms of the reference atmosphere and is equivalent to the air density ratio defined in appendix B. Sensitivities of the analytical vibration modes to the simulated shaker mass are shown in table II and figure 17, and the modes with the shaker mass included are compared with experimentally determined vibration modes at near vacuum in figure 16. Virtual mass effects of air pressure on the analytical vibration modes are discussed in appendix B according to the approximation illustrated in figure 18. Results of this approximation are shown in figures 19 and 20.

Test Results

Out-of-plane vibration modes were found at resonant frequencies ranging from 13.94 to 99.71 Hz. Figures 9 to 12 show natural frequencies and corresponding mode shapes (indicated by dashed-curve node patterns) at various values of cable tension. Most experimental mode shapes in figures 9 to 12 were obtained from sinusoidal force inputs and are generally in fair agreement with modes obtained by the random-force-

input methods. Response frequencies by the different test methods tended to agree better than mode shapes. Four modes for which the nodal pattern depended most on test method are shown in figure 10.

The restrictions of noise level, along with the low damping of the membrane and small air-pressure fluctuations, made modal identification difficult, particularly by the ITD random-input method. The long sampling times chosen for the random input forces, 4 minutes for each of the 130 test measurement points, were not always sufficient to obtain reliable modal data. The frequencies not identified for some tensions in figures 9 to 11 and the variations in both nodal patterns and frequencies in figure 10 are attributed to the sensitivity of the vibration data to low input forces.

Tension effects.- Variation in tension at the membrane apexes from 89 to 262 N (20 to 59 lb) resulted in linear trends of the square of the frequency with tension as shown in figure 13. For subsequent correlation with analytical vibration modes, experimental modes are classified as symmetric or antisymmetric, wherever possible, according to their response-amplitude directions with respect to the vertical centerline of the membrane. The higher order modes in figure 13(b) are not readily identifiable from the nodal patterns of figure 11 as symmetric or antisymmetric. Experimental resonant frequencies increased with increasing tension, as expected, without significant mode-shape changes. The nodal pattern of figure 10(b) is indicative of the differences encountered in mode shape. Another form of mode-shape deviation attributable to tension is indicated by the reversed nodal pattern of the sixth mode (f = 43.85 and 67.77) in figure 11.

The linear trends in figure 13 indicate that for each vibration mode, there is a constant value of the ratio f^2/T which can be used to estimate the natural frequencies of a geometrically similar structure of the same materials as the present model. As shown in appendix A, this estimate is based on two requirements: (1) that a dimensionless eigenvalue formed from this ratio be identical in both membranes and (2) that both membranes experience the same strain. From these requirements, tension at the apex is found to scale as the square of a geometric scale factor, and frequency as the inverse of the scale factor. Thus, a three-sided Mylar membrane geometrically similar and 3 times larger will have frequencies approximately one-third those of the present model and apex tensions 9 times larger.

Effects of air-pressure variation.- Figure 14 shows the effects of ambient air pressure on frequencies and maximum response amplitudes measured at two points. These frequencies and amplitudes can, for the first few modes, be identified with the nodal patterns previously shown. Response frequencies and amplitudes increase in varying amounts with decreasing air pressure, with higher modes having the largest increases at lowest pressures. Considerable complexity in responses is evident at middle to high frequencies and at midpressure levels, where diminishing response peaks suggest the existence of nodes close to points A and B and the coupling of mode shapes with similar frequencies. The frequencies from the analysis shown by the triangle symbols along the abscissa of figure 14(a) are discussed later.

Comparisons of test results show significantly lower and more closely spaced frequencies at atmospheric pressure (figs. 11 and 12), with mode shapes more distorted than at near vacuum (fig. 9). Moreover, there is clearly an alteration in the sequence of identifiable modes, with the seventh mode in figure 9 becoming the fourth mode in figures 11 and 12. The first mode has modal response amplitudes which bulge

in the membrane central surface more at 1 atm (fig. 11) and 0.610 atm (fig. 12) than at 0.008 to 0.018 atm (fig. 9). Such comparisons indicate the sensitivity of membrane vibrations to air pressure and associated virtual mass effects.

The effect of air-pressure variations on damping is shown in figure 15. Values of structural damping coefficient g associated with response peaks for probe position A (based on fig. 14(a)) are shown for various air pressures and vibration modes. These results indicate the membrane to be a lowly damped structure, with structural damping coefficients ranging from 0.2 to 1.4 percent. Damping coefficients at very low pressures are generally lower and reasonable measures of structural damping without air-damping contributions.

Analytical Results

The SPAR analysis was used to calculate both symmetric and antisymmetric resonant frequencies and mode shapes for specified tensile preloads and thermal strain compensations. Analytical results are presented in tables II and III and figures 13(a), 16, and 17. Results in table IV are discussed in appendix B and show effects of nonstructural air-mass approximations (fig. 18) on frequency and mode shape (figs. 19 and 20).

Results for the three arrangements of grid points of figure 7 are compared in table II and show convergence. Omission of the thermal strain compensation, which is needed to obtain uniform membrane stresses, had a negligible effect on most of the analytical vibration modes. The largest effect was a 6.8-percent reduction in the frequency of the symmetric mode with the near-circular node. In addition, there was no effect of constraining the axial displacements of the extended cable ends, other than to eliminate all but one of the in-plane vibration modes (not presented) from within the out-of-plane frequency spectrum.

Table III and figure 17 show the effects of the localized rigid mass simulating moving parts of the electrodynamic shaker. Neglect of this mass results in omission of the third symmetric mode and alteration in the shape of the fourth symmetric mode, as shown in figure 17(b). This mass was considered a necessary input to the SPAR analysis to obtain a truer representation of the shaker effect on the experimental vibration modes.

Comparison of Test and Analytical Results

Analytical vibration modes obtained with the 154-grid-point model are compared with test results for the near-vacuum condition in figures 13(a), 14(a), and 16. Figure 16 shows calculated frequencies and mode shapes (as solid curves marking node locations) for three tension values. Omitted frequencies are denoted by dashed curves. The analytical modes are in fair agreement with the experimental modes. Experimental modes that are antisymmetric with respect to the vertical centerline consistently agree better than do symmetric modes. This trend is also evident in figure 13(a) over the complete tension range.

Resemblances are noted in the nodal patterns of certain modes found in this study with those found in references 2 and 3. Despite differences in boundary conditions between the present model and the triangular models of references 2 and 3, similarities are evident for modes identified in figure 13(a) as 1st, 2nd, and 5th symmetric and 1st, 2nd, and 3rd antisymmetric.

CONCLUDING REMARKS

Studies of out-of-plane vibration modes have been carried out in a vacuum chamber for a three-sided aluminized Mylar membrane with inwardly curved edges. Uniform tension was transmitted by thin steel cables encased in the edges and leading from the three apexes, to which moderate tension loads were applied.

Linear trends of squared natural frequency (up to 100 Hz) with moderate tension level, 89 to 262 N (20 to 59 lb), are useful for projecting results from this model to other dynamically similar membranes by means of simple relations.

Significant effects on membrane vibration modes were found from varying air pressure in the vacuum chamber. Variation of ambient air pressure from atmospheric to near vacuum caused significant increases in dynamic response amplitudes and frequencies. These frequencies became more closely spaced and the mode shapes became more highly coupled as the ambient air pressure increased to atmospheric. The first few vibration modes measured at near vacuum are shown to be predictable by finite-element structural analysis. However, further work is desirable to quantify the air effects.

The membrane structure was found to have low damping, with structural damping coefficients less than 1.4 percent regardless of surrounding air pressure. This low damping, together with sensitivity of the vibration modes to low noise-level force inputs and small air-pressure fluctuations, made modal identification difficult.

Langley Research Center
National Aeronautics and Space Administration
Hampton, VA 23665
November 16, 1982

APPENDIX A

STRUCTURAL DYNAMIC SIMILARITY

This appendix shows how the constant ratios indicated by the linear trends in figure 13 may be used to estimate parameters of other geometrically and structurally scaled cable-tensioned membranes. These estimates can be made by means of simple geometric scale factors obtained from principles of dynamic and structural similarity, involving the invariance of two sets of dimensionless parameters determined independently.

One of these sets of parameters includes a dimensionless eigenvalue, which may be written as a general function of four other dimensionless parameters. In obtaining this relation, the frequency $\omega = 2\pi f$ for any vibration mode may be expressed by

$$\omega = F_1(T, \rho_m, \rho_c, t, R, L, d) \tag{A1}$$

in terms of the general function F_1 of apex tension T, membrane and cable mass densities ρ_m and ρ_c, and geometrical features that include membrane thickness t, edge radius R, representative length L, and cable diameter d. These seven variables and ω may be defined in terms of the three fundamental units of length, time, and mass to form five (eight minus three) dimensionless parameters in accordance with Buckingham's pi theorem. (See refs. 19 to 22.) Four of these parameters are simple ratios evolving by inspection or physical insight as ρ_c/ρ_m, t/L, R/L, and d/L. The fifth one is a dimensionless eigenvalue $\frac{\omega^2 \rho_m L^4}{T}$, which may be obtained by a formal dimensional analysis procedure involving ω, ρ_m, L, and T expressed in a product of length, mass, and time units to different powers that are determined by solving simultaneous equations (ref. 20, e.g.). Thus, equation (A1) may be rewritten as

$$\frac{\omega^2 \rho_m L^4}{T} = \bar{F}_1\left(\frac{\rho_c}{\rho_m}, \frac{t}{L}, \frac{R}{L}, \frac{d}{L}\right) \tag{A2}$$

which is unaffected by scale effects (i.e., changes in the magnitudes of the three fundamental units) and is therefore valid for the model of the present study and any other geometrically scaled cable-tensioned membrane. The conditions of dynamic and structural similarity (as stipulated in ref. 21, e.g.) require that the ratios in the rewritten general function $\bar{F}_1$ be identical for both models. Consequently, the dimensionless eigenvalue on the left side of equation (A2) will also have identical values in both models.

With L_P/L_M taken as λ, the scale factor, these similarity conditions may be expressed by the following equations:

$$\left(\frac{\rho_c}{\rho_m}\right)_M = \left(\frac{\rho_c}{\rho_m}\right)_P \tag{A3}$$

$$\left(\frac{t}{L}\right)_M = \left(\frac{t}{L}\right)_P = \frac{t_P}{L_M \lambda}$$

whence

$$\frac{t_P}{t_M} = \lambda \tag{A4a}$$

$$\left(\frac{R}{L}\right)_M = \left(\frac{R}{L}\right)_P = \frac{R_P}{L_M \lambda}$$

whence

$$\frac{R_P}{R_M} = \lambda \tag{A4b}$$

$$\left(\frac{d}{L}\right)_M = \left(\frac{d}{L}\right)_P = \frac{d_P}{L_M \lambda}$$

whence

$$\frac{d_P}{d_M} = \lambda \tag{A4c}$$

$$\left(\frac{\omega^2 \rho_m L^4}{T}\right)_M = \left(\frac{\omega^2 \rho_m L^4}{T}\right)_P = \left(\frac{\omega^2 \rho_m}{T}\right)_P L_M^4 \lambda^4 \tag{A5}$$

where the subscript M denotes the model and the subscript P denotes a prototype geometrically scaled from the model. If both structures are made of the same materials, then, from equation (A3),

$$(\rho_m)_M = (\rho_m)_P \tag{A6a}$$

and

$$(\rho_c)_M = (\rho_c)_P \tag{A6b}$$

and equation (A5) reduces to

$$\left(\frac{\omega^2}{T}\right)_M = \left(\frac{\omega^2}{T}\right)_P \lambda^4 \tag{A7}$$

which clearly requires knowledge of a scale factor for tension in order to obtain a frequency scale factor.

The scale factor for tension may be determined from the invariance of a second set of dimensionless parameters, with T included in a strain parameter, which may be written as a general function of four other dimensionless parameters. This relation may be obtained from

$$T = F_2(E_m, \mu_m, E_c, t, R, d) \tag{A8}$$

where F_2 is a general function of six variables that include E_m and E_c, Young's moduli for the membrane and cable, and μ_m, Poisson's ratio for the membrane. Since none of the variables in this equation are time-dependent, the number of fundamental units for the dimensional variables can be reduced from three to two, namely, length and force. Then, again according to Buckingham's theorem, five dimensionless parameters may be identified. Four of these are, by inspection, $\frac{E_c}{E_m}$, μ_m, $\frac{t}{R}$, and $\frac{d}{R}$. The fifth one, $\frac{T}{E_m R^2}$, is a general strain, which may also be obtained by the procedure of reference 20 from the solution for the exponents of T, E_m, and R expressed in a product of length and force units to different powers. Then equation (A8) may be written as

$$\frac{T}{E_m R^2} = \bar{F}_2\left(\frac{E_c}{E_m}, \mu_m, \frac{t}{R}, \frac{d}{R}\right) \tag{A9}$$

which, as for equation (A2), is also unaffected by scale effects. Thus, values of the dimensionless parameters must for similarity be the same for the model M and the geometrically scaled counterpart P, so that

$$\left.\begin{aligned}\left(\frac{E_c}{E_m}\right)_M &= \left(\frac{E_c}{E_m}\right)_P \\ (\mu_m)_M &= (\mu_m)_P\end{aligned}\right\} \qquad \text{(A10)}$$

$$\left.\begin{aligned}\left(\frac{t}{R}\right)_M &= \left(\frac{t}{R}\right)_P \\ \left(\frac{d}{R}\right)_M &= \left(\frac{d}{R}\right)_P\end{aligned}\right\} \qquad \text{(A11)}$$

$$\left(\frac{T}{E_m R^2}\right)_M = \left(\frac{T}{E_m R^2}\right)_P \qquad \text{(A12)}$$

For the same materials in both models,

$$\left.\begin{aligned}(E_m)_M &= (E_m)_P \\ (\mu_m)_M &= (\mu_m)_P \\ (E_c)_M &= (E_c)_P\end{aligned}\right\} \qquad \text{(A13)}$$

and, using the scale factor for R from equation (A4b), the scale factors for t and d are the same as before in equations (A4a) and (A4c). Equation (A12) then reduces to

$$\frac{T_M}{R_M^2} = \frac{T_P}{R_M^2 \lambda^2} \qquad \text{(A14)}$$

from which

$$\frac{T_P}{T_M} = \lambda^2$$

With the scale factor for tension known, equation (A7) becomes

$$\frac{\omega_M^2}{T_M} = \frac{\omega_P^2}{T_M \lambda^2} \lambda^4 = \frac{\omega_P^2}{T_M} \lambda^2$$

from which the scale factor for frequency is found to be

$$\frac{\omega_P}{\omega_M} = \frac{1}{\lambda} \tag{A15}$$

This is the well-known factor previously derived for other geometrically and dynamically similar structures involving bending and made from the same materials.

As noted in reference 23, this kind of modeling is valid as long as strain-rate effects (i.e., millimeter per millimeter per second) are negligible, as is true for most conventional structural materials. While the effects of strain-rate variations on the structural properties of thin Mylar are unknown to the authors, in-plane membrane displacements due to the maximum tension loads for the present investigation appear to be well within the linear range of the load-deformation test curves in reference 24. On this basis, Mylar strain-rate effects are not expected to be significant.

The dimensionless eigenvalue and strain parameters in equations (A2) and (A9) are general expressions that could have been made specific without changing the resulting scale factors. An actual functional form of $\bar{F}_1$ in equation (A2) could have been obtained by some linear combination of dimensionless eigenvalues of membrane and cable. Likewise, a specific form of $\bar{F}_2$ in equation (A9) could have been obtained by a linear combination of equations (4) in the main text.

APPENDIX B

ANALYTICAL APPROXIMATION OF AMBIENT-AIR EFFECTS

The effects of ambient air on membrane out-of-plane vibration modes were approximated as a nonstructural mass contained within a curved envelope surface defined as shown in figure 18 over one planform surface of the membrane. The envelope surface is the locus of quarter circles lying in vertical planes normal to the membrane edge and containing the membrane element centroids. The radius r_i of each quarter circle is the distance from the membrane edge to the nearest of the three symmetry axes. In each vertical plane, the element centroid is located by the coordinate ξ_i which, together with r_i, determines the distance z_i of the envelope surface from the membrane, as shown in figure 18. The corresponding local mass per unit area m_i is then computed and input to the SPAR vibration analysis as nonstructural mass. Air-mass contributions from both planform surfaces of the membrane are represented by the factor 2 in m_i.

Frequencies and mode shapes calculated by this approximation, using the SPAR model of figure 7(c), are presented in table IV and figures 19 and 20 for 102 N (23 lb) of tension. Results to simulate 1 atm are presented in the first column of table IV and in figure 19. Frequencies for this condition are lower than test frequencies in figure 11. The first-mode frequency is within 9.5 percent of the test value, and the central bulge in the mode shape is predicted fairly well. Frequencies of higher modes tend to be closely spaced, as do experimental frequencies, but lack agreement by as much as 27 percent for identifiable modes. Analytical mode shapes correlate somewhat better with test mode shapes than do analytical and test frequencies for the first four modes.

Results obtained using air-mass loadings of 80, 61, and 42 percent of the air mass at 1 atm are shown in the second, third, and fourth columns of table IV and in figure 20. Air-mass reductions are equivalent to air-density reductions ρ_{a_r}/ρ_{a_1}, where ρ_{a_r} is the air-mass density at a partial atmosphere and ρ_{a_1} is the air-mass density at 1 atm.

Frequencies were increased with no appreciable change in corresponding mode shapes for the first four modes. However, large mode-shape alterations were found for certain higher modes, as shown in figure 20. Despite the crude nature of the air-mass approximation, the frequency trends in table IV and figure 20 and the higher order mode-shape changes are similar to the complicated modal response behavior indicated in figure 14.

A rigorous mathematical treatment of this effect would require application of acoustic radiation theory, such as that developed by Pretlove in reference 25 for deriving a generalized air mass and by Irgens and Brand in reference 26 for air damping as well as the air-mass effects. Such an effort is outside the scope of the present study.

REFERENCES

1. Agrawal, Pradeep K.; Anderson, Melvin S.; and Card, Michael F.: Preliminary Design of Large Reflectors With Flat Facets. IEEE Trans. Antennas & Propag., vol. AP-29, no. 4, July 1981, pp. 688-694.

2. Irie, Toshihiro; Yamada, Gen; and Umesato, Kazuo: Free Vibration of Regular Polygonal Plates With Simply Supported Edges. J. Acoust. Soc. America, vol. 69, no. 5, May 1981, pp. 1330-1336.

3. Evensen, David A.: Vibration Analysis of Multi-Symmetric Structures. AIAA Paper No. 75-808, May 1975.

4. Laura, Patricio A.; and Faulstich, Albert J., Jr.: An Application of Conformal Mapping to the Determination of the Natural Frequency of Membranes of Regular Polygonal Shape. Developments in Mechanics, Volume 3 - Part 2: Dynamics and Fluid Mechanics, T. C. Huang and M. W. Johnson, Jr., eds., John Wiley & Sons, Inc., 1965, pp. 155-163.

5. Bettess, Peter: Eigenvalues for $\Delta\phi + \lambda\phi = 0$ in Regular Polygons. J. Eng. Mech. Div., American Soc. Civil Eng., vol. 106, no. EM6, Dec. 1980, pp. 1433-1438.

6. Nagaya, K.: Dynamic Response of a Membrane With Both Curved and Straight Line Boundaries. Trans. ASME, J. Appl. Mech., vol. 46, no. 3, Sept. 1979, pp. 667-671.

7. Nagaya, K.: Vibration of an Arbitrarily Shaped Membrane With Point Supports. J. Sound & Vib., vol. 65, no. 1, July 8, 1979, pp. 1-9.

8. Williams, R.; Yeow, Y. T.; and Brinson, H. F.: An Analytical and Experimental Study of Vibrating Equilateral Triangular Plates. Exp. Mech., vol. 15, no. 9, Sept. 1975, pp. 339-346.

9. Whetstone, W. D.: SPAR Structural Analysis System Reference Manual. System Level 13A. Volume 1: Program Execution. NASA CR-158970-1, 1978.

10. Knapp, Karl; and Hedgepeth, John: Study of Membrane Reflector Technology. ARC-TN-1071 (Contract No. 955081), Astro Research Corp., Jan. 2, 1979. (Available as NASA CR-158729.)

11. Dielectric Breakdown Problems With Space Hardware. Insulation, Apr. 1969, p. 17.

12. Stahle, Clyde V.: Modal Test Methods and Applications. J. Environ. Sci., vol. 21, no. 1, Jan./Feb. 1978, pp. 24, 33-35.

13. Kennedy, Charles C.; and Pancu, C. D. P.: Use of Vectors in Vibration Measurement and Analysis. J. Aeronaut. Sci., vol. 14, no. 11, Nov. 1947, pp. 603-625.

14. Schoenster, James A.; and Clary, Robert R.: Experimental Investigation of the Longitudinal Vibration of a Representative Launch Vehicle With Simulated Propellants. NASA TN D-4502, 1968.

15. Scanlan, Robert H.; and Rosenbaum, Robert: Introduction to the Study of Aircraft Vibration and Flutter. Macmillan Co., c.1951.

16. Richardson, Mark; and Potter, Ron: Identification of the Modal Properties of an Elastic Structure From Measured Transfer Function Data. Instrumentation in the Aerospace Industry - Volume 20, Advances in Test Measurement - Volume 11, Proceedings of the 20th International Instrumentation Symposium, Inst. Soc. America, 1974, pp. 239-246.

17. Pappa, Richard S.; and Ibrahim, Samir R.: A Parametric Study of the Ibrahim Time Domain Modal Identification Algorithm. Shock & Vib. Bull., no. 51, Pt. 3, May 1981, pp. 43-72.

18. Ibrahim, Samir R.; and Pappa, Richard S.: Large Modal Survey Testing Using the Ibrahim Time Domain (ITD) Identification Technique. AIAA-81-0528, Apr. 1981.

19. Buckingham, E.: On Physically Similar Systems; Illustrations of the Use of Dimensional Equations. Phys. Rev., ser. 2, vol. IV, no. 4, Oct. 1914, pp. 345-376.

20. Bridgman, P. W.: Dimensional Analysis. Yale Univ. Press, 1922.

21. Goodier, J. N.; and Thomson, W. T.: Applicability of Similarity Principles to Structural Models. NACA TN No. 933, 1944.

22. Bisplinghoff, Raymond L.; Ashley, Holt; and Halfman, Robert L.: Aeroelasticity. Addison-Wesley Pub. Co., Inc., c.1955, pp. 695-704.

23. Abramson, H. Norman; and Nevill, Gale E., Jr.: Some Modern Developments in the Applications of Scale-Models in Dynamic Testing. Use of Models and Scaling in Shock and Vibration, Wilfred E. Baker, ed., American Soc. Mech. Eng., c.1963, pp. 1-15.

24. Hinson, W. F.; and Goslee, J. W.: Uniaxial and Biaxial Tensioning Effects on Thin Membrane Materials. NASA TM-81812, 1980.

25. Pretlove, A. J.: Note on the Virtual Mass for a Panel in an Infinite Baffle. J. Acoust. Soc. America, vol. 38, no. 2, Aug. 1965, pp. 266-270.

26. Irgens, F.; and Brand, R. S.: Coupling of Acoustic Fields and Vibrating Membranes and Plates. Contracts NONR 2512(00) and N 70024-68-C-0070, Mech. Eng. Dept., Univ. of Connecticut, July 1, 1968. (Available from DTIC as AD 837 966.)

TABLE I.- STRUCTURAL PROPERTIES OF THREE-SIDED MEMBRANE

Mylar membrane
$E = 3.4$ GPa $(0.489 \times 10^6$ psi$)$
$\mu = 0.3$
$\alpha = 2.7 \times 10^{-6} \frac{\text{mm}}{\text{mm}/^\circ\text{C}} \left(1.5 \times 10^{-6} \frac{\text{in.}}{\text{in.}/^\circ\text{F}}\right)$
$\rho = 1384 \text{ kg/m}^3 \left(1.294 \times 10^{-4} \frac{\text{lb-sec}^2}{\text{in}^4}\right)$
$t = 0.0127$ mm $(0.0005$ in.$)$
$R = 1.41$ m $(55.5$ in.$)$
Steel cable
$E = 165.5$ GPa $(24.0 \times 10^6$ psi$)$
$\mu = 0.3$
$\alpha = 1.4 \times 10^{-5} \frac{\text{mm}}{\text{mm}/^\circ\text{C}} \left(8.0 \times 10^{-6} \frac{\text{in.}}{\text{in.}/^\circ\text{F}}\right)$
$\rho = 5500 \text{ kg/m}^3 \left(5.142 \times 10^{-4} \frac{\text{lb-sec}^2}{\text{in}^4}\right)$
$d = 1.60$ mm $(0.063$ in.$)$

TABLE II.- VIBRATION-MODE RESULTS FOR GRID VARIATIONS OF SPAR MODEL AT 102 N (23 LB) APEX TENSION

Frequency, Hz			Mode-shape description
124 grid points	138 grid points	154 grid points	
28.38	28.33	28.38	Symmetric overall response without nodes
40.50	40.50	40.51	Symmetric with one lateral node
41.08	40.99	41.09	Antisymmetric (about vertical centerline)
57.06	57.03	57.05	Symmetric with two widely separated lateral nodes
65.98	65.95	65.95	Antisymmetric with two nodes and responses in four quadrants of model
71.47	71.38	71.49	Symmetric with two inwardly curved nodes, and one lateral node close to shaker location
80.10	79.82	80.43	Symmetric with overall near-circular node
80.86	80.79	80.80	Antisymmetric with nodes 60° apart intersecting at membrane center
98.29	98.17	98.36	Symmetric with inwardly curved node along each edge of model

TABLE III.- EFFECT OF SHAKER MASS SIMULATION ON VIBRATION-MODE RESULTS CALCULATED FROM SPAR AT 93 N (21 LB) APEX TENSION

[154-grid-point model]

Frequency, Hz		Mode-shape description
With shaker mass	Without shaker mass	
27.12	27.30	Symmetric overall response without nodes
38.71	39.24	Symmetric with one lateral node
39.26	39.26	Antisymmetric (about vertical centerline)
54.52		Symmetric with two widely separated lateral nodes (see also fig. 17)
63.02	63.02	Antisymmetric with two nodes and responses in four quadrants
68.31	63.02	Symmetric with two inwardly curved nodes[a]
76.83	75.32	Symmetric with overall near-circular node[a]
77.21	77.21	Antisymmetric with nodes 60° apart intersecting at membrane center
93.98	92.34	Symmetric with inwardly curved node along each edge of model[a]

[a]Additional node close to bottom apex. (See also fig. 17.)

TABLE IV.- EFFECTS OF APPROXIMATE AIR MASS ON VIBRATION MODES CALCULATED FROM SPAR AT 102 N (23 LB) APEX TENSION

Frequency, Hz				Mode-shape description
$\frac{\rho_{a_r}}{\rho_{a_1}} = 1.00$ (*)	$\frac{\rho_{a_r}}{\rho_{a_1}} = 0.80$ (*)	$\frac{\rho_{a_r}}{\rho_{a_1}} = 0.61$ (*)	$\frac{\rho_{a_r}}{\rho_{a_1}} = 0.42$ (*)	
12.73	14.00	15.62	18.00	Symmetric overall response without nodes
23.09	25.27	27.94	31.49	Symmetric with one lateral node
23.26	25.45	28.14	31.74	Antisymmetric (about vertical centerline)
27.36	29.48	32.01	35.50	Symmetric with central overall near-circular node
34.83	38.07	41.70**	46.63**	Symmetric with circular node in lower central part of model and lateral node across upper part of model
34.92	38.21	41.95	47.02	Antisymmetric with two nodes and responses in four quadrants of model
36.93	40.02**	44.30**	50.50**	Symmetric (fig. 20)
37.31	40.45	44.81	51.73**	Antisymmetric with central vertical and upper circular nodes
41.86	45.32	49.85**	56.59**	Symmetric (fig. 20)

*$\rho_{a_1} = 1.2256\ kg/m^3 \left(1.147 \times 10^{-7}\ \frac{lb\text{-}sec^2}{in^4}\right)$.

**Changed mode shape (fig. 20).

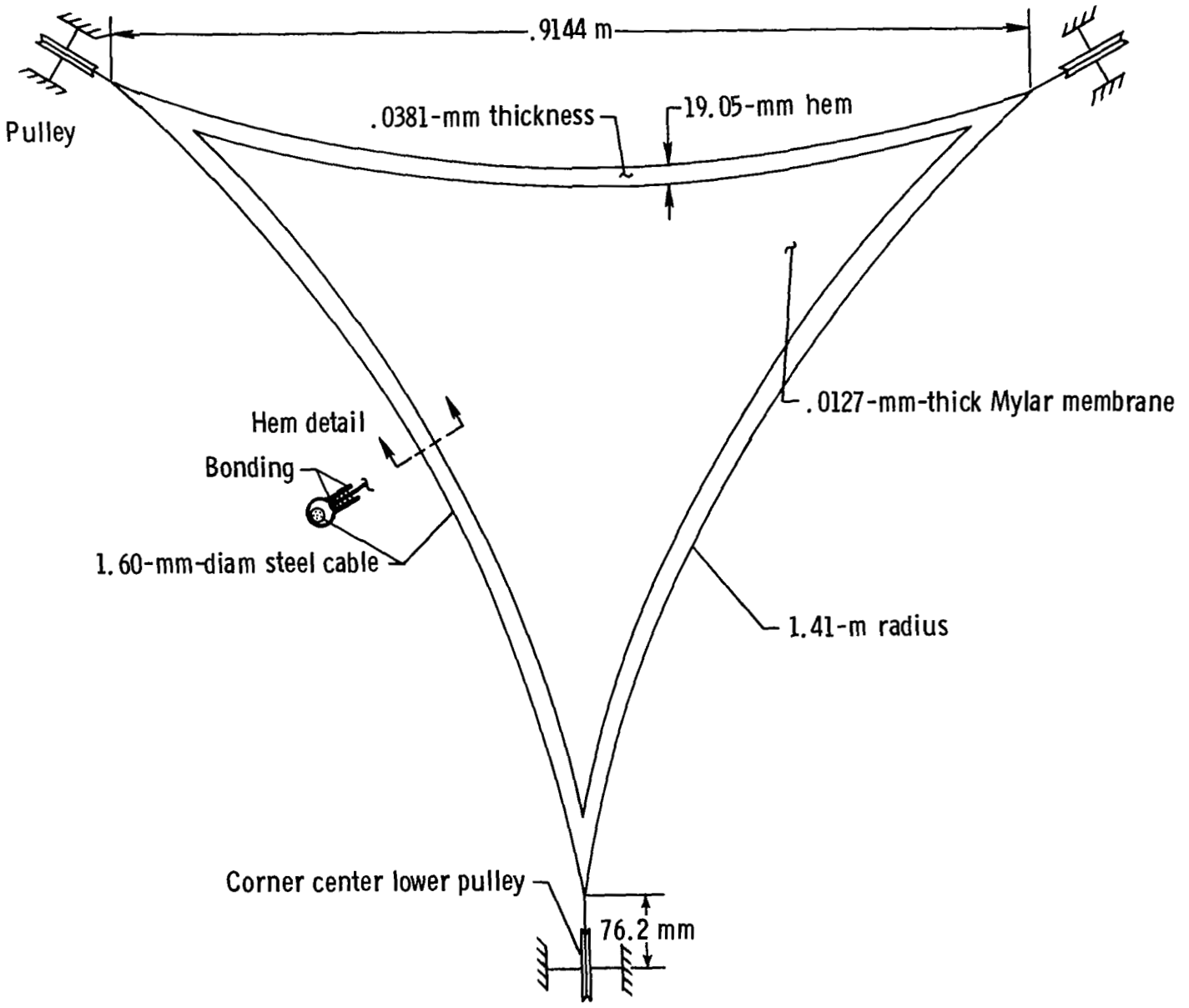

Figure 1.- Three-sided membrane model.

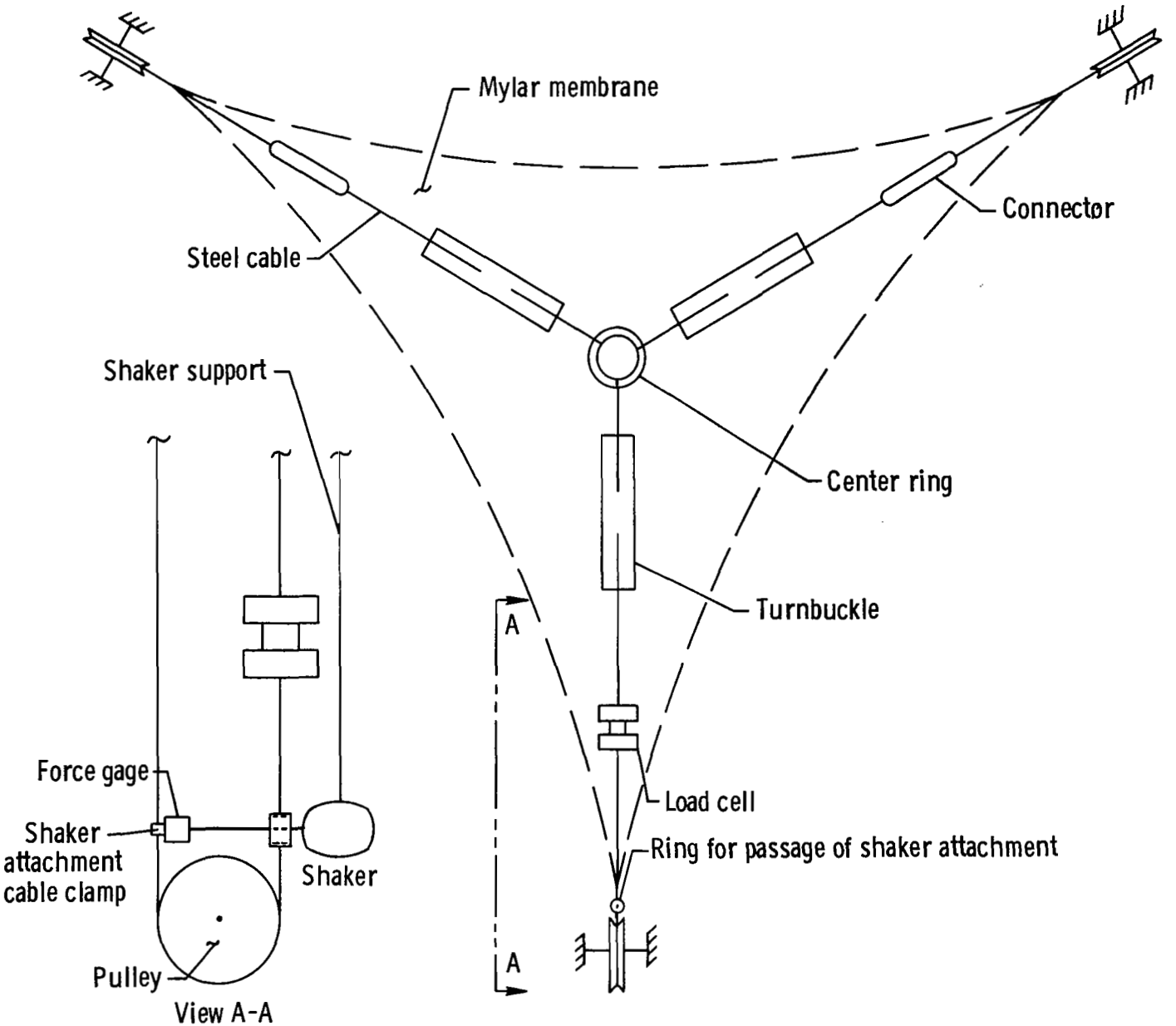

Figure 2.- Schematic of back-surface support structure for three-sided membrane; manual tension control.

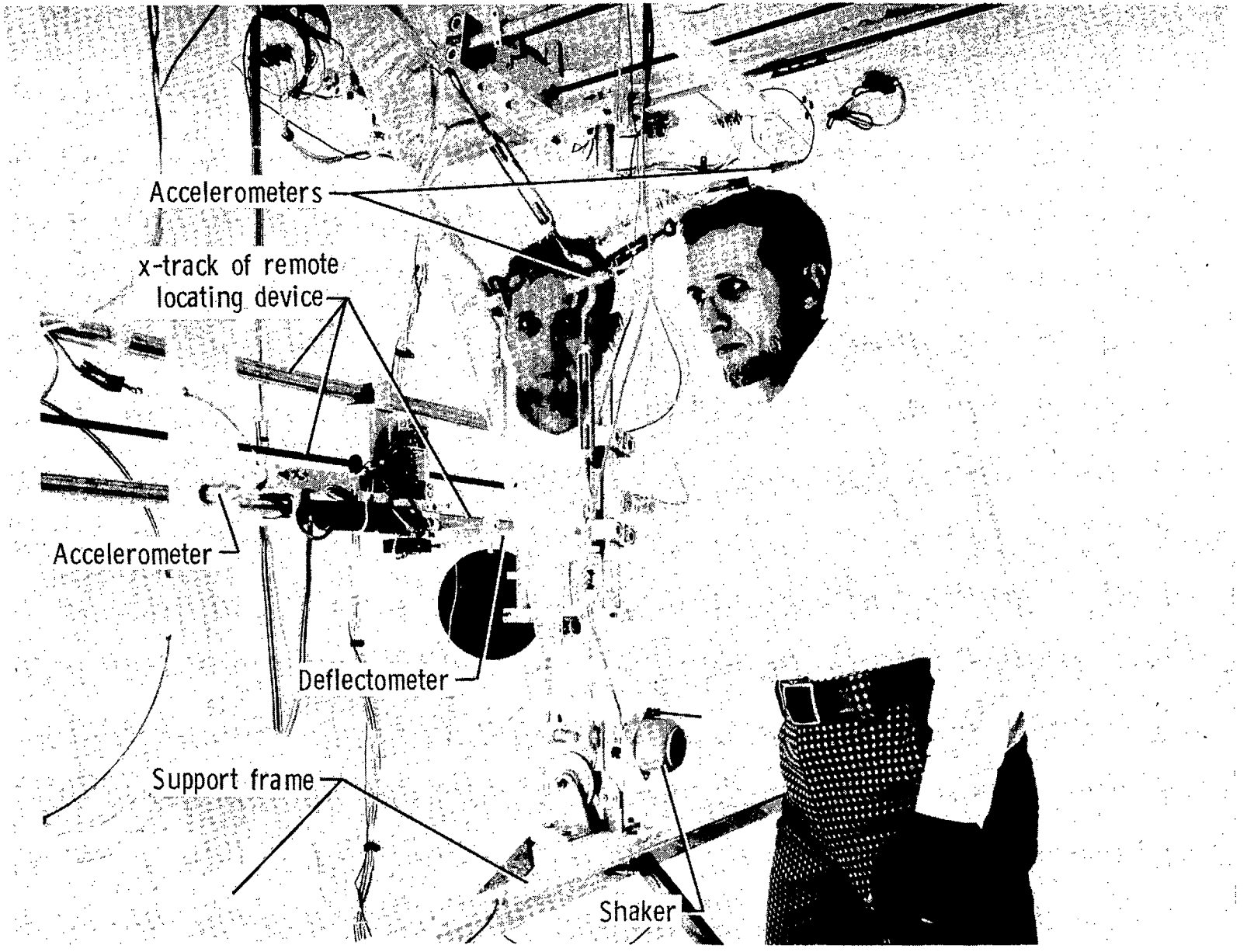

L-80-8005

Figure 3.- Three-sided membrane and test apparatus mounted in 8-foot-diameter spherical vacuum chamber.

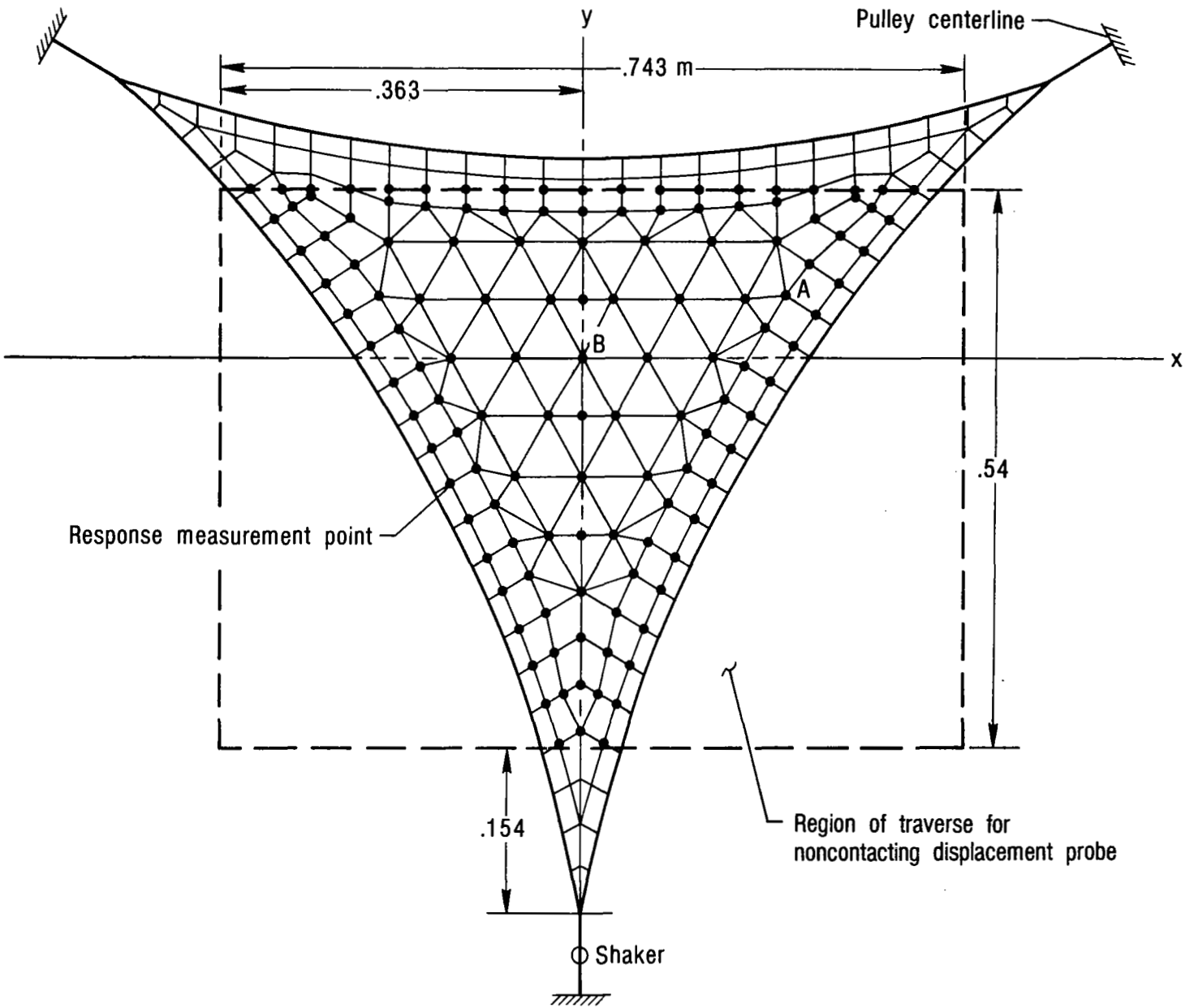

Figure 4.- Locations of modal survey measurement. Dots denote 130 measurement points on 248-grid-point SPAR model (fig. 7(a)).

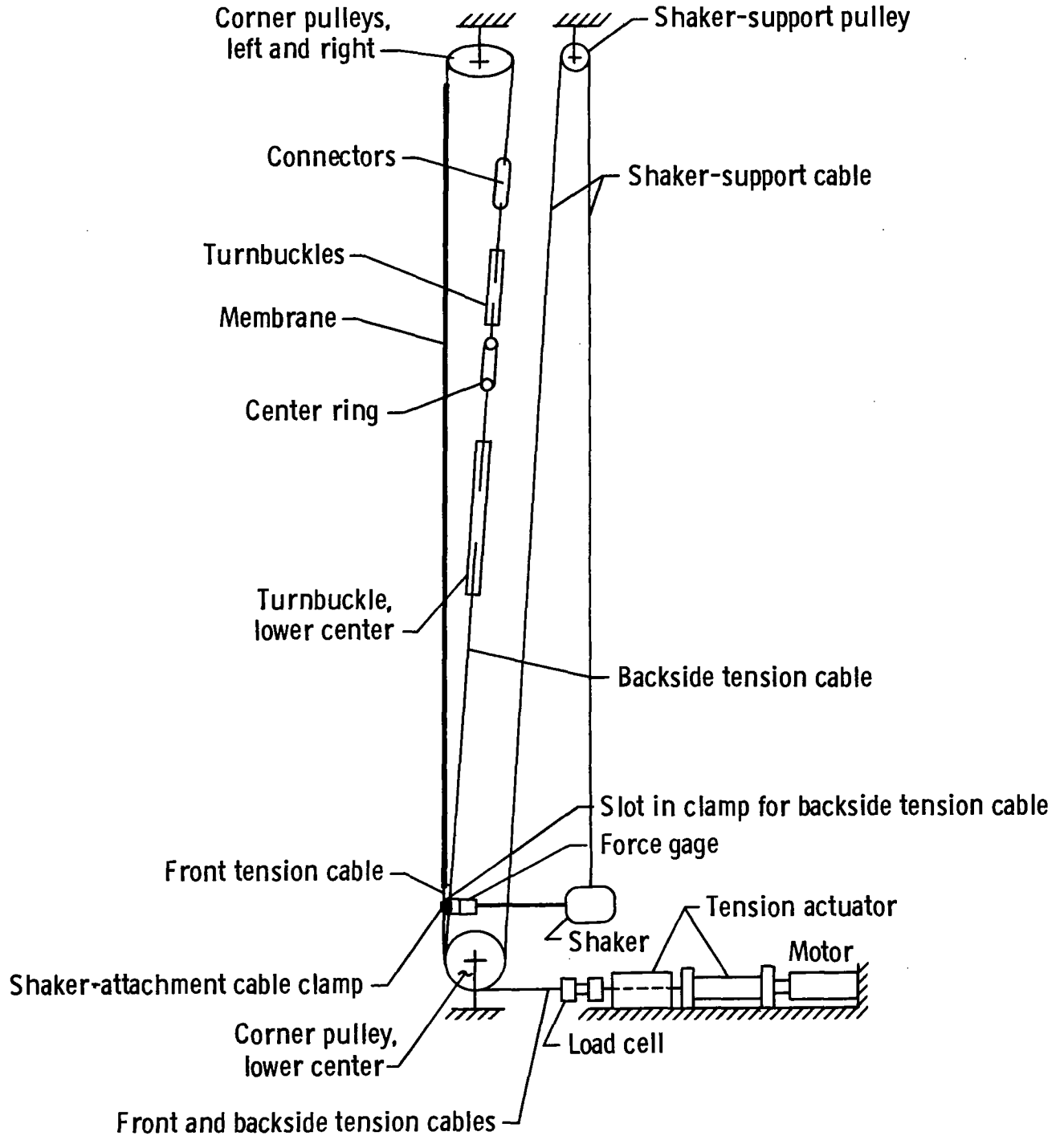

(a) Schematic.

Figure 5.- Test apparatus modified for automated tension control. Shaker and force gage are clamped to front and shaker-support cables.

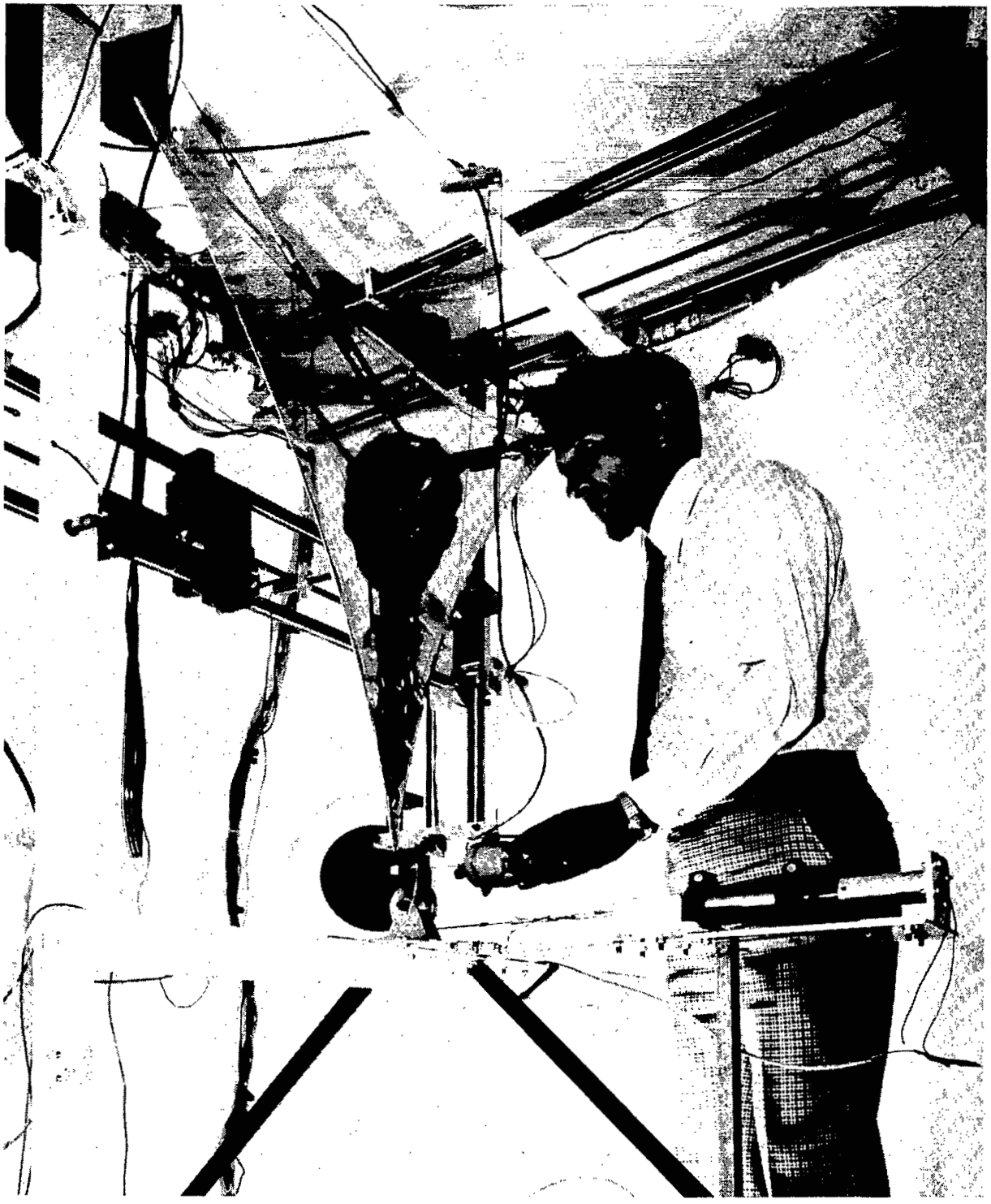

L-81-4382

(b) Overall view in test chamber.

Figure 5.- Concluded.

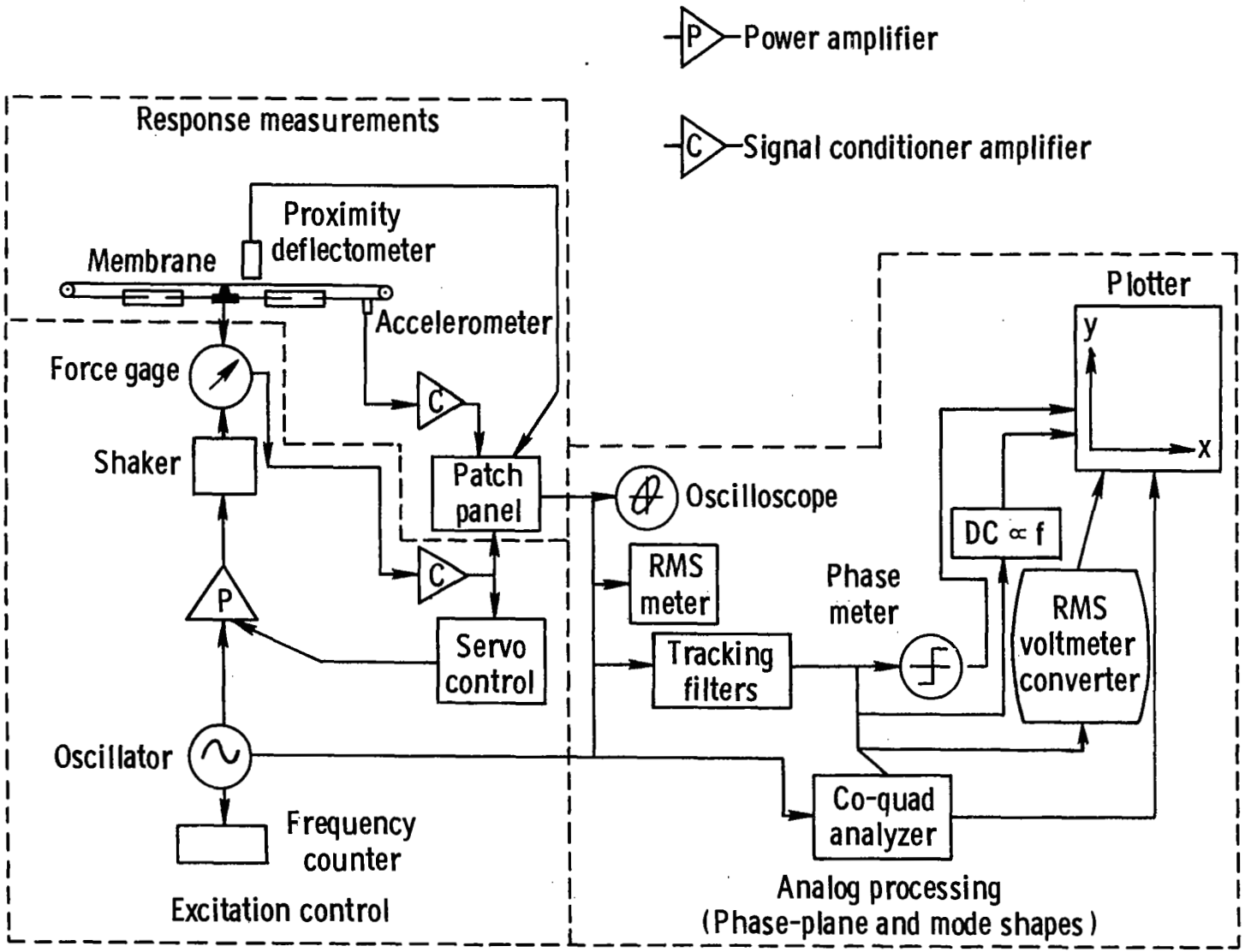

(a) Sinusoidal input.

Figure 6.- Flow charts of vibration tests for sinusoidal and random inputs.

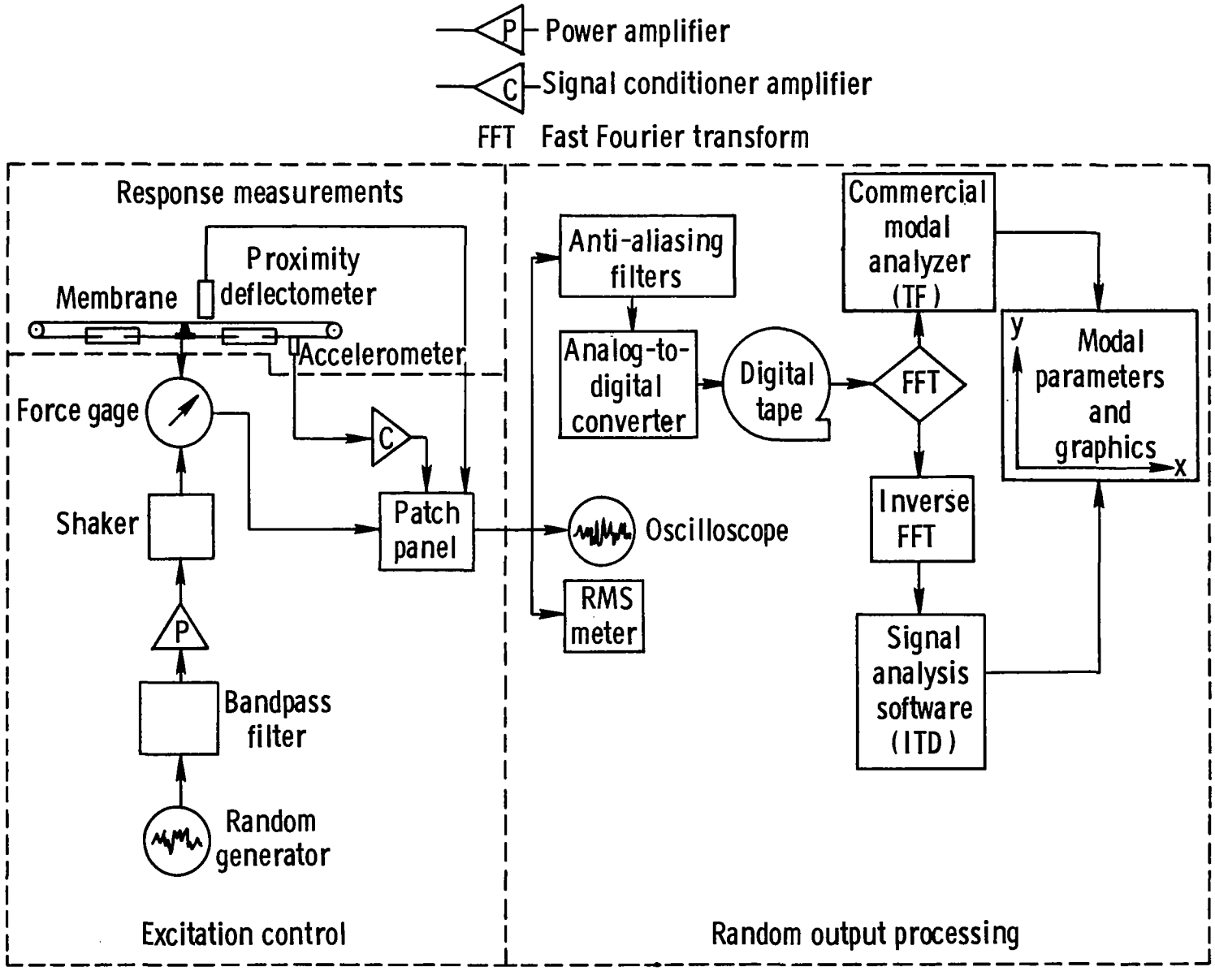

(b) Random input, with output processed by transfer function (TF) or Ibrahim time domain (ITD) methods.

Figure 6.- Concluded.

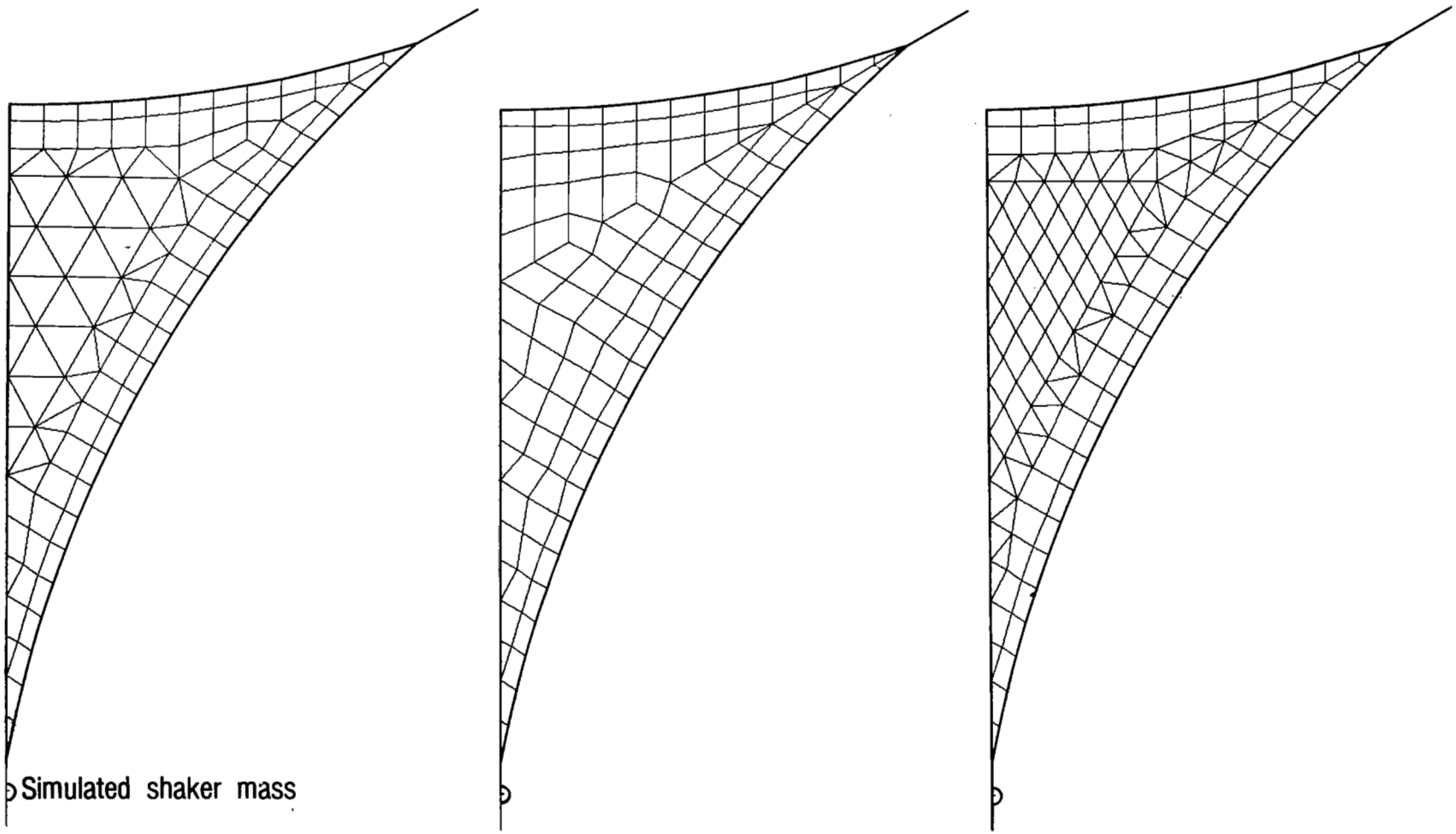

(a) 124 grid points (b) 138 grid points. (c) 154 grid points.

Figure 7.- SPAR half models of three-sided membrane.

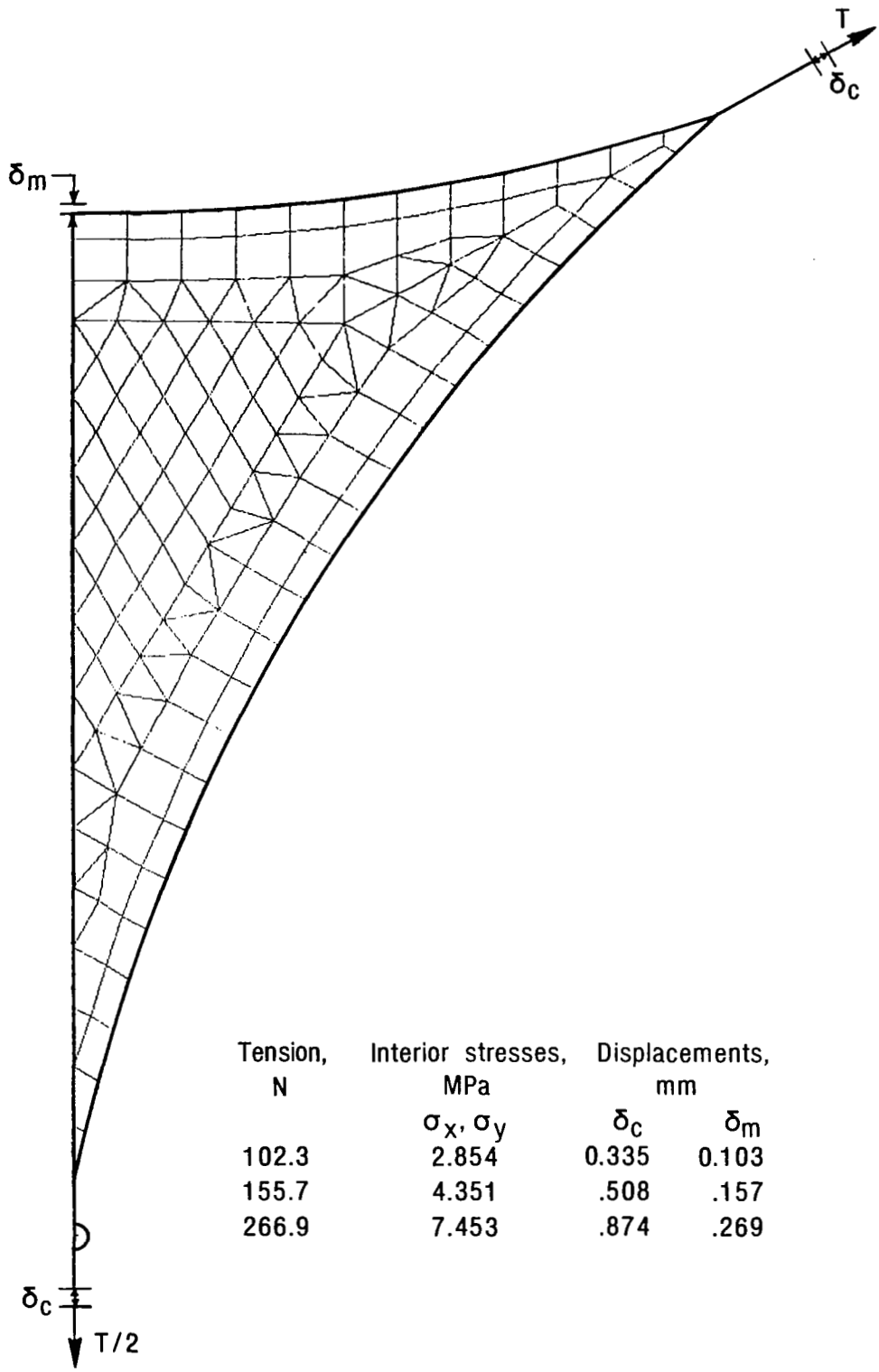

Tension, N	Interior stresses, MPa	Displacements, mm	
	σ_x, σ_y	δ_c	δ_m
102.3	2.854	0.335	0.103
155.7	4.351	.508	.157
266.9	7.453	.874	.269

Figure 8.- SPAR static stresses and displacements.

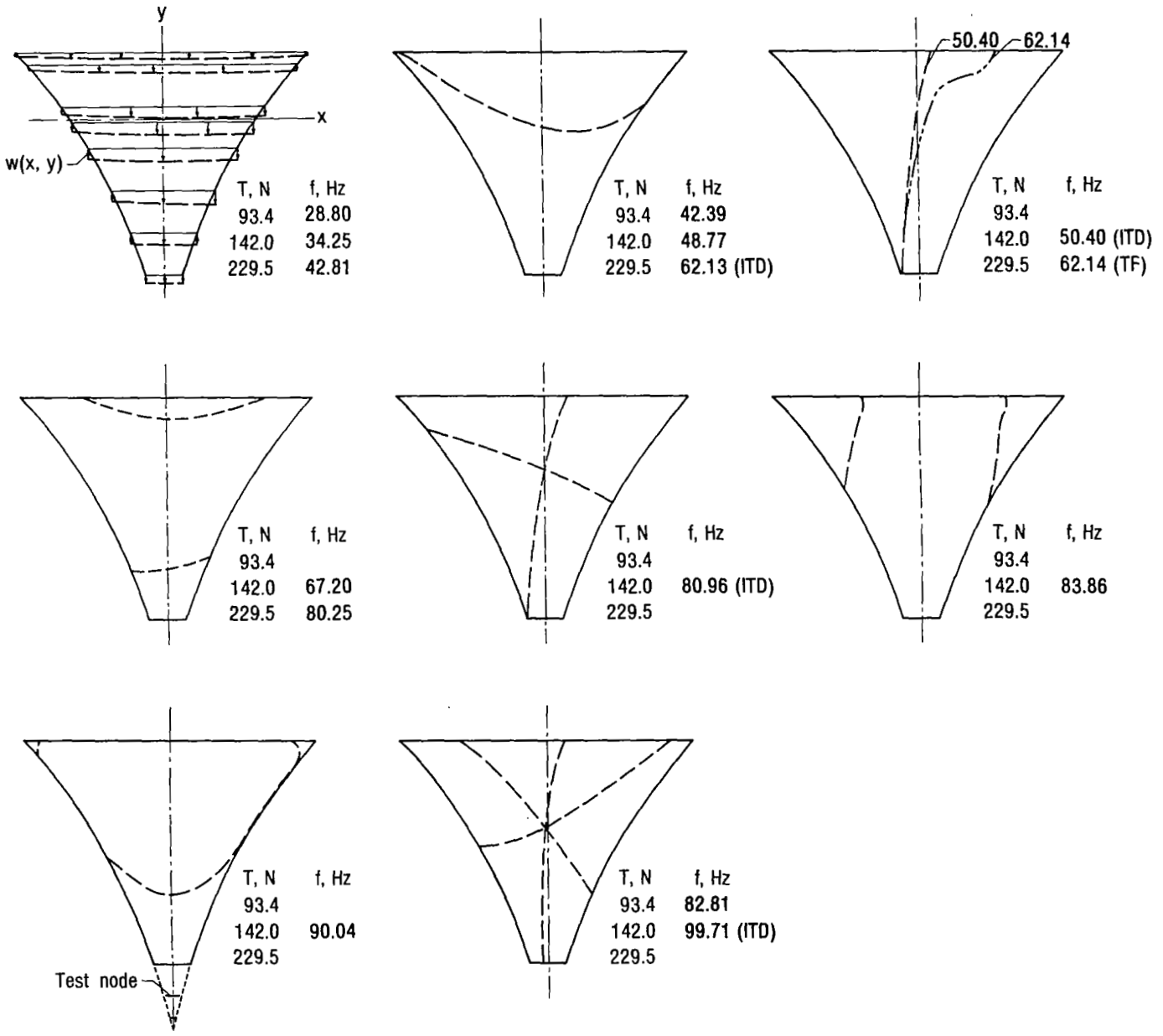

Figure 9.- Membrane experimental vibration modes in near vacuum of 0.008 to 0.018 atm under equal apex tension loads. All data are obtained by sinusoidal input unless otherwise specified.

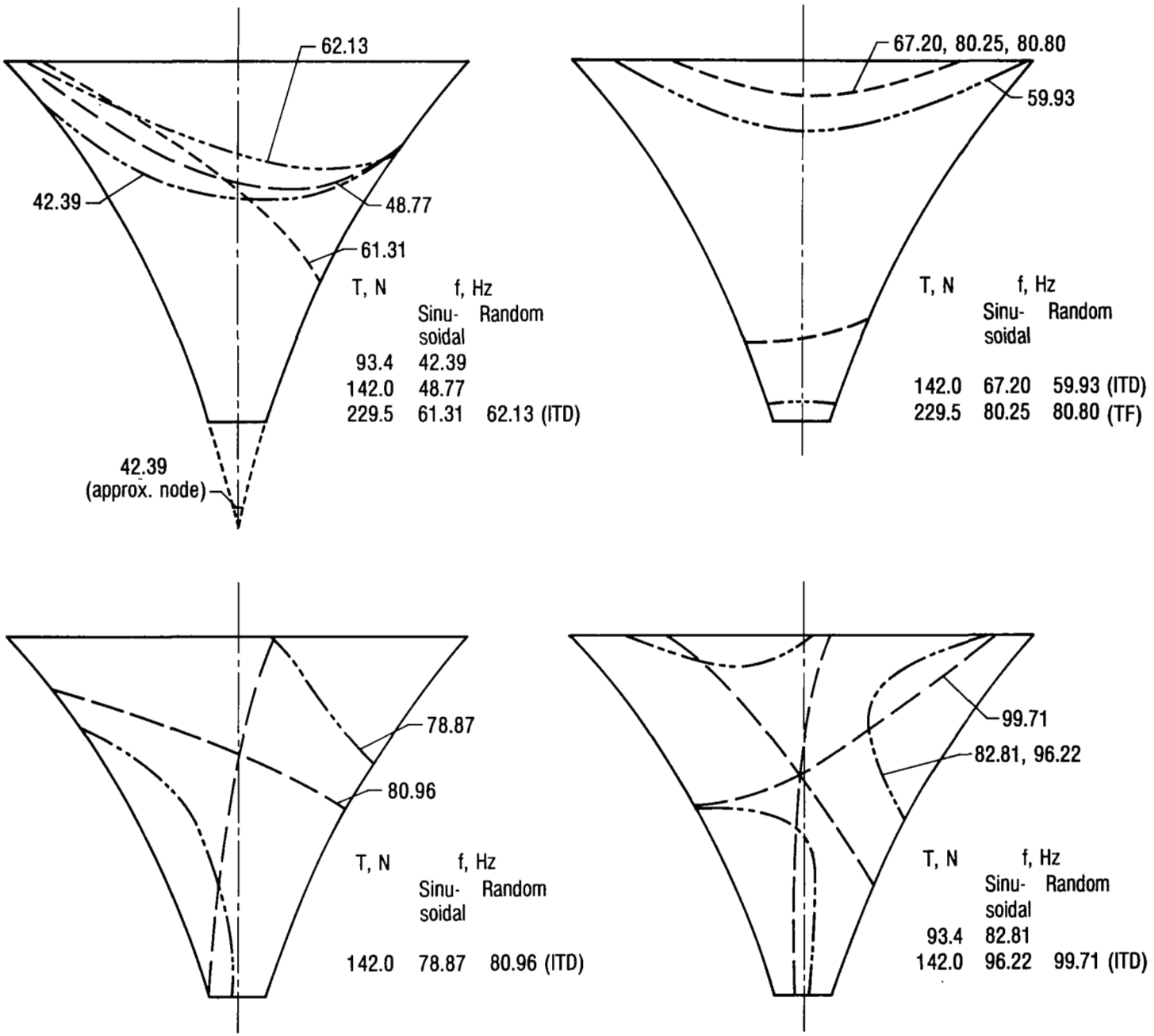

Figure 10.- Selected membrane-experimental-mode comparisons showing differences due to excitation method and tension variation at 0.008 to 0.018 atm.

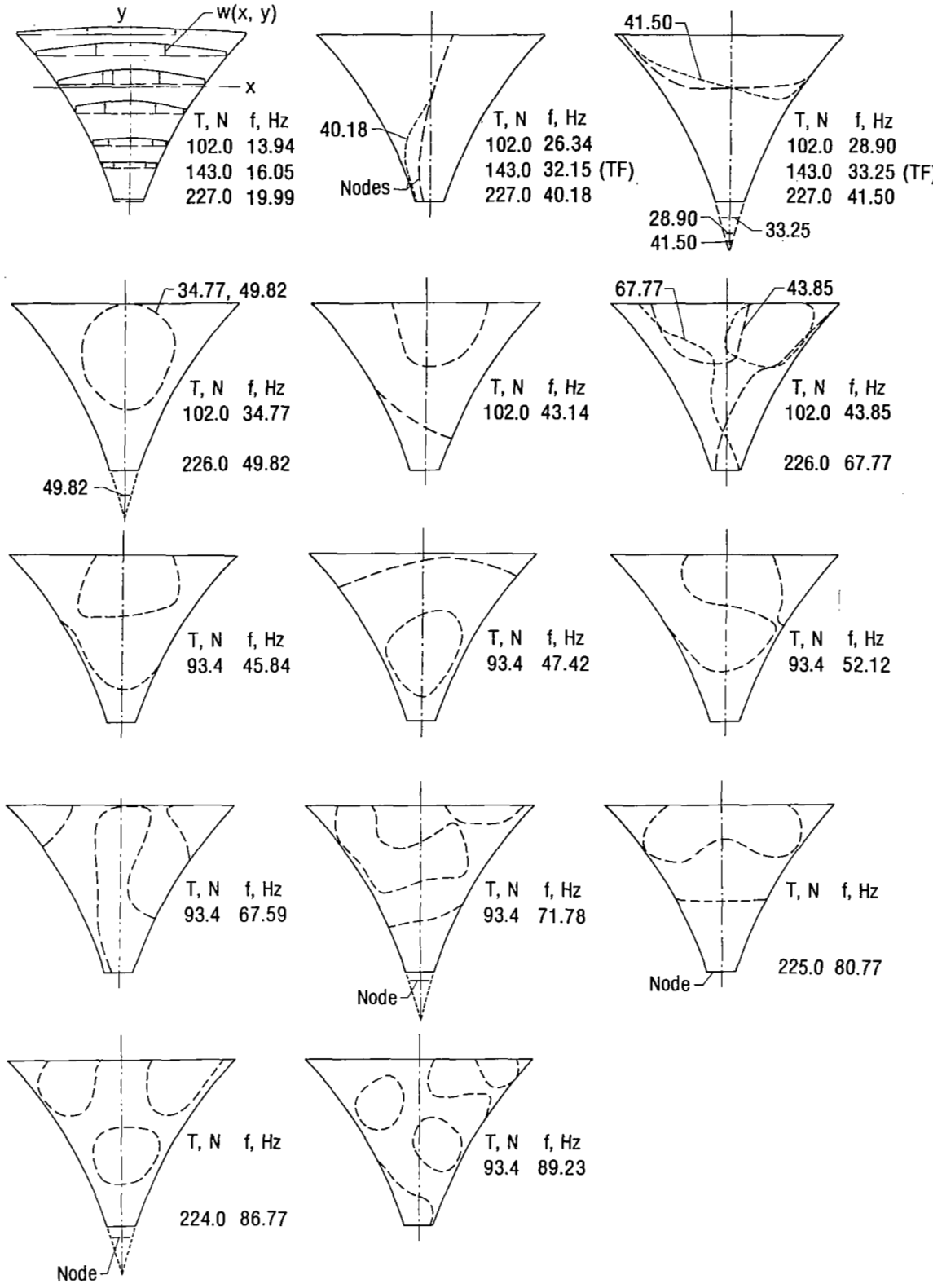

Figure 11.- Membrane experimental vibration modes at 1 atm under equal apex tension loads. All data are obtained by sinusoidal input unless otherwise specified.

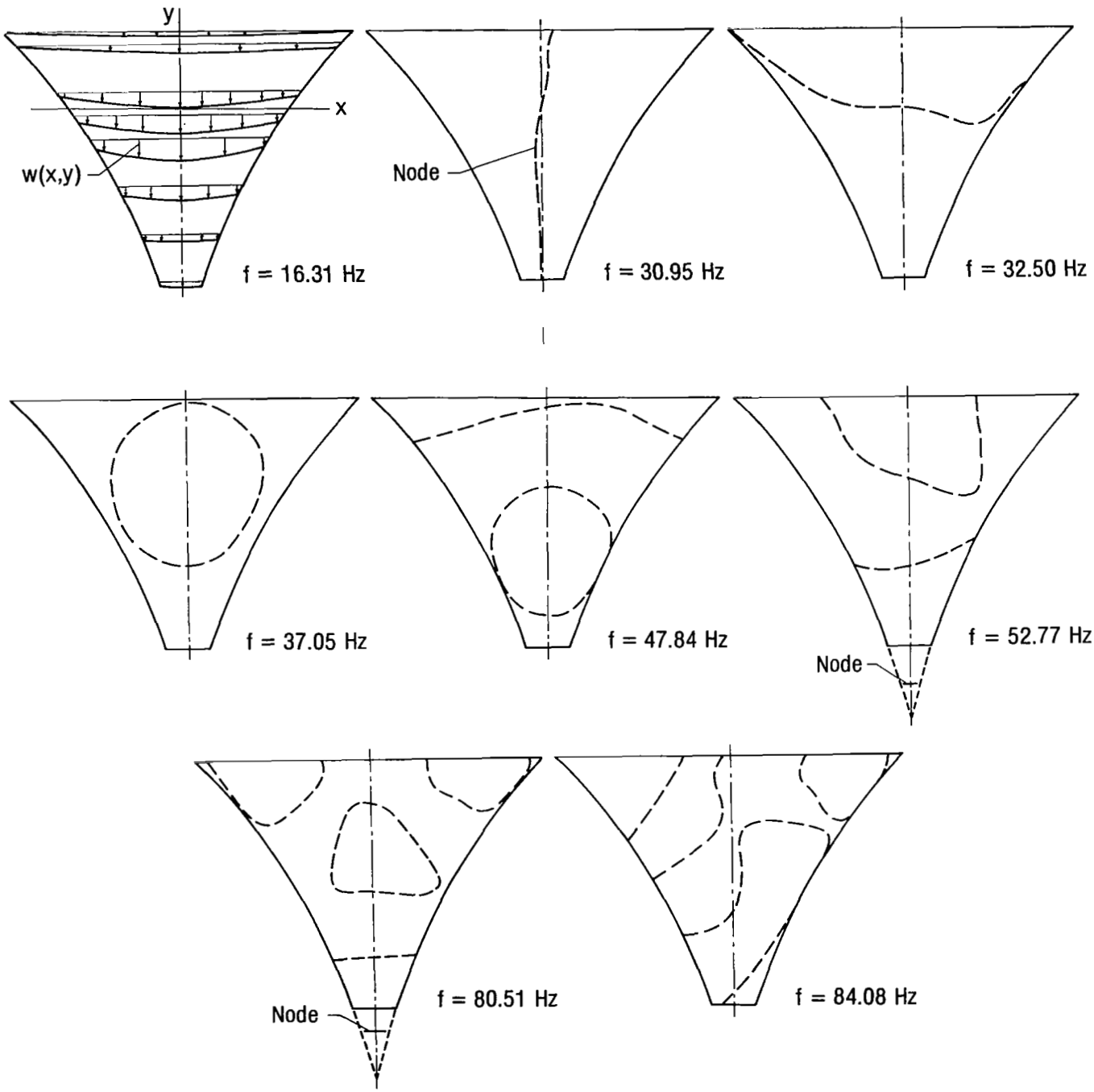

Figure 12.- Membrane experimental vibration modes at 93.4 N (21 lb) under equal apex tension at 0.61 atm by sinusoidal input.

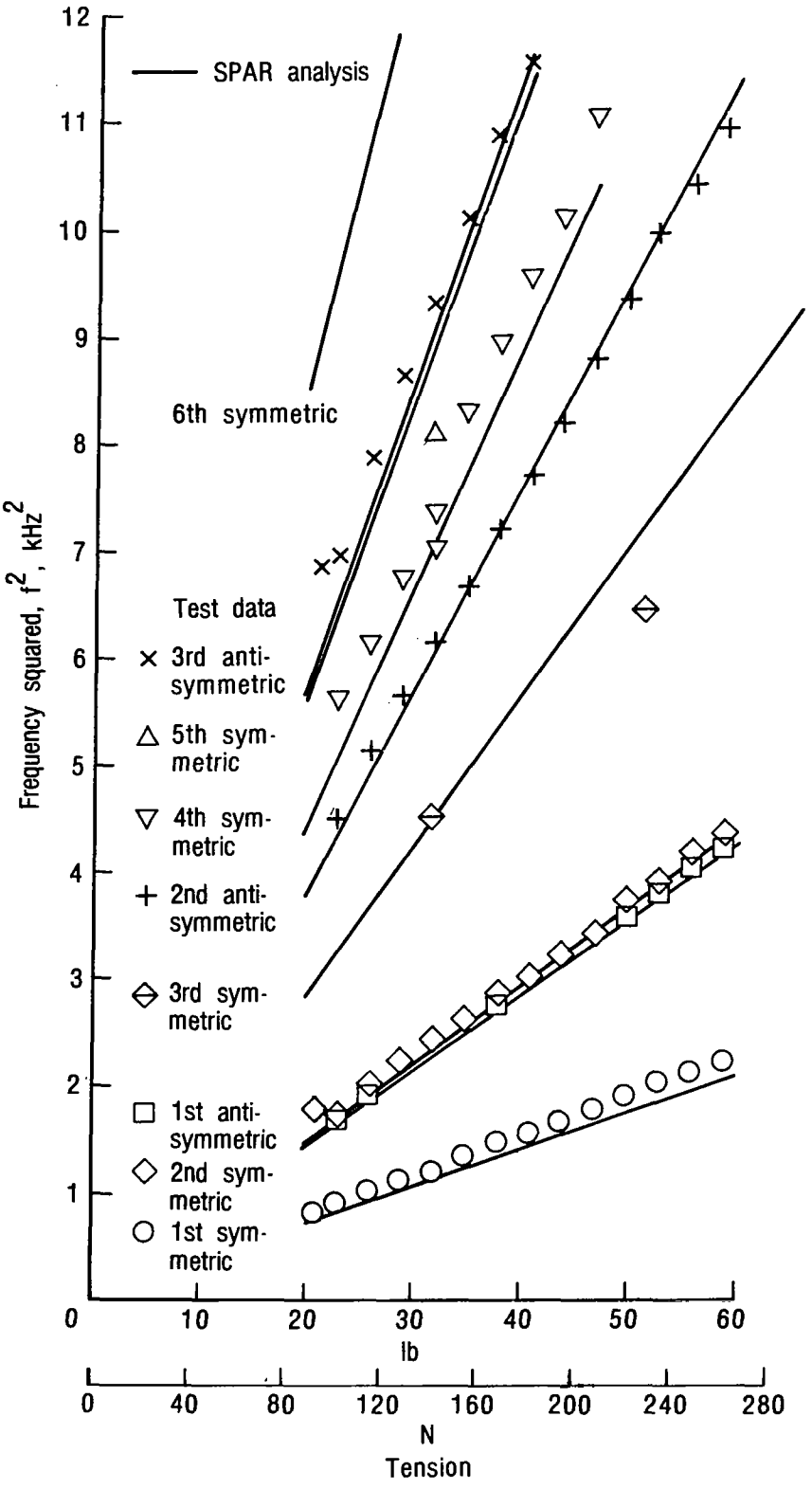

(a) In near vacuum of 0.011 to 0.018 atm.

Figure 13.- Variations of the square of membrane frequencies with apex tension.

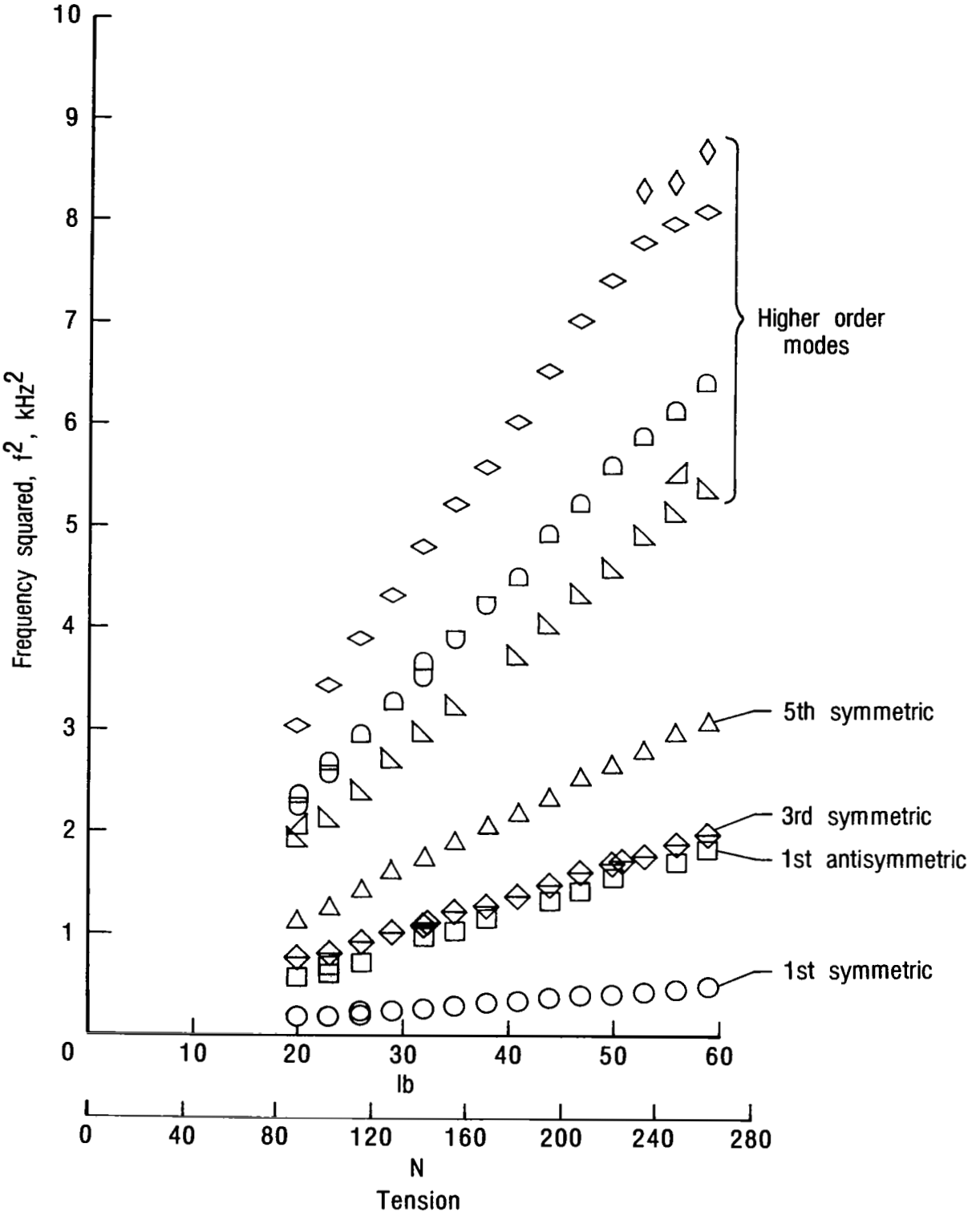

(b) In air at 1.0 atm.

Figure 13.- Concluded.

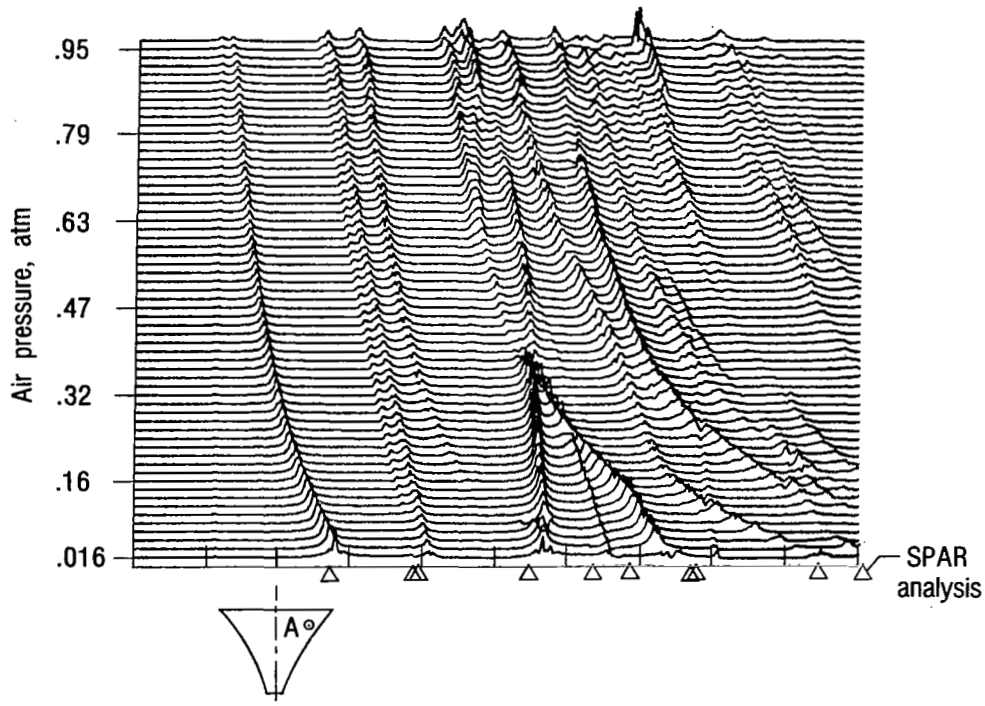

(a) Response displacements at point A.

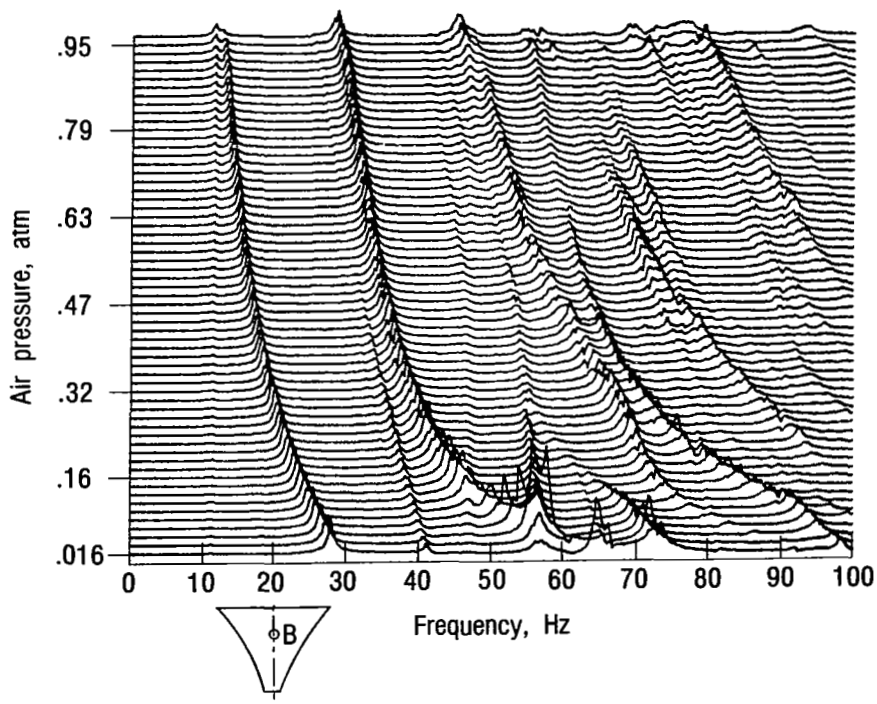

(b) Response displacements at point B.

Figure 14.- Response-displacement variations with air pressure and frequency measured by random-input method (TF) with 93.4 N (21 lb) apex tension.

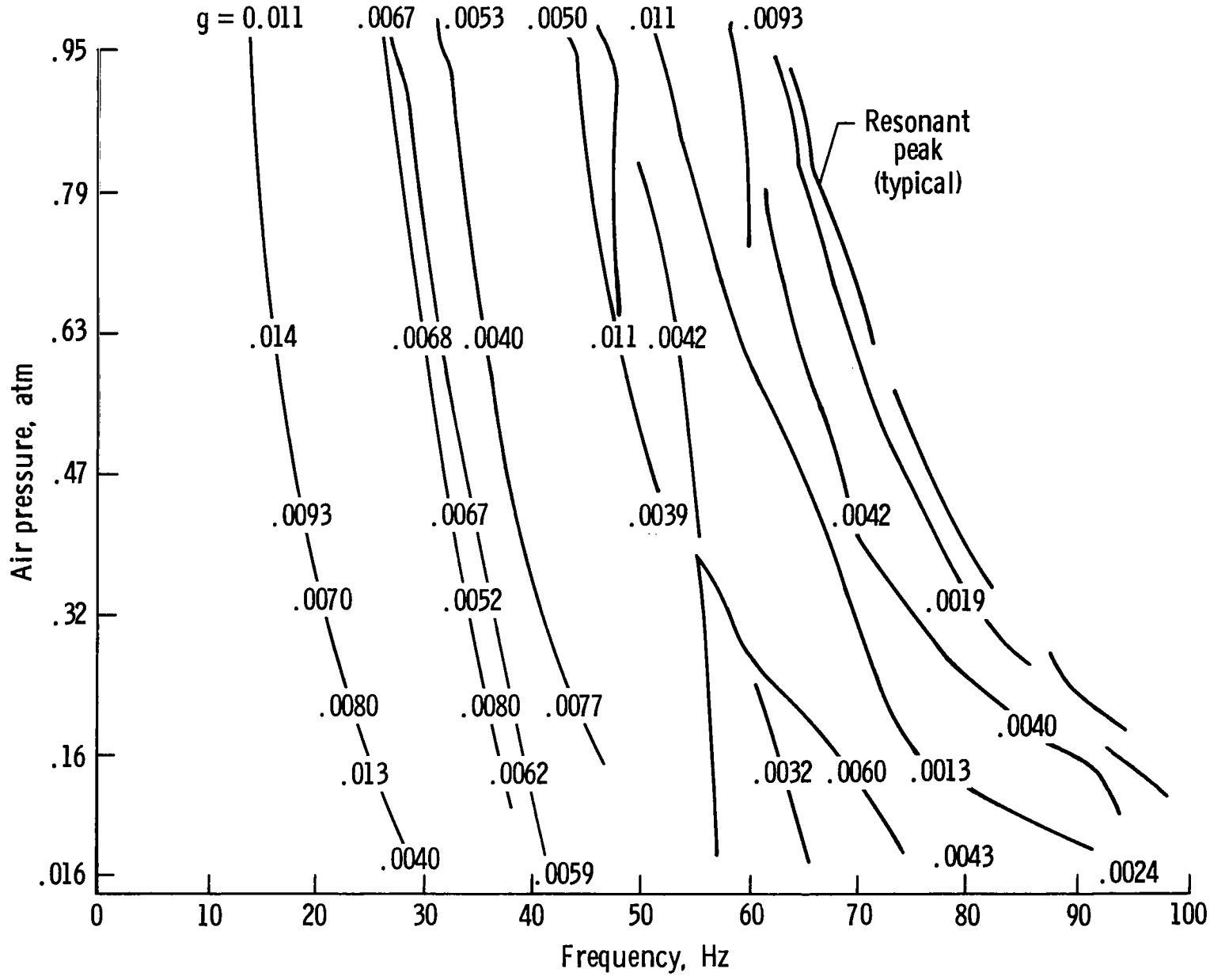

Figure 15.- Structural damping coefficients for 93.4 N (21 lb) apex tension.

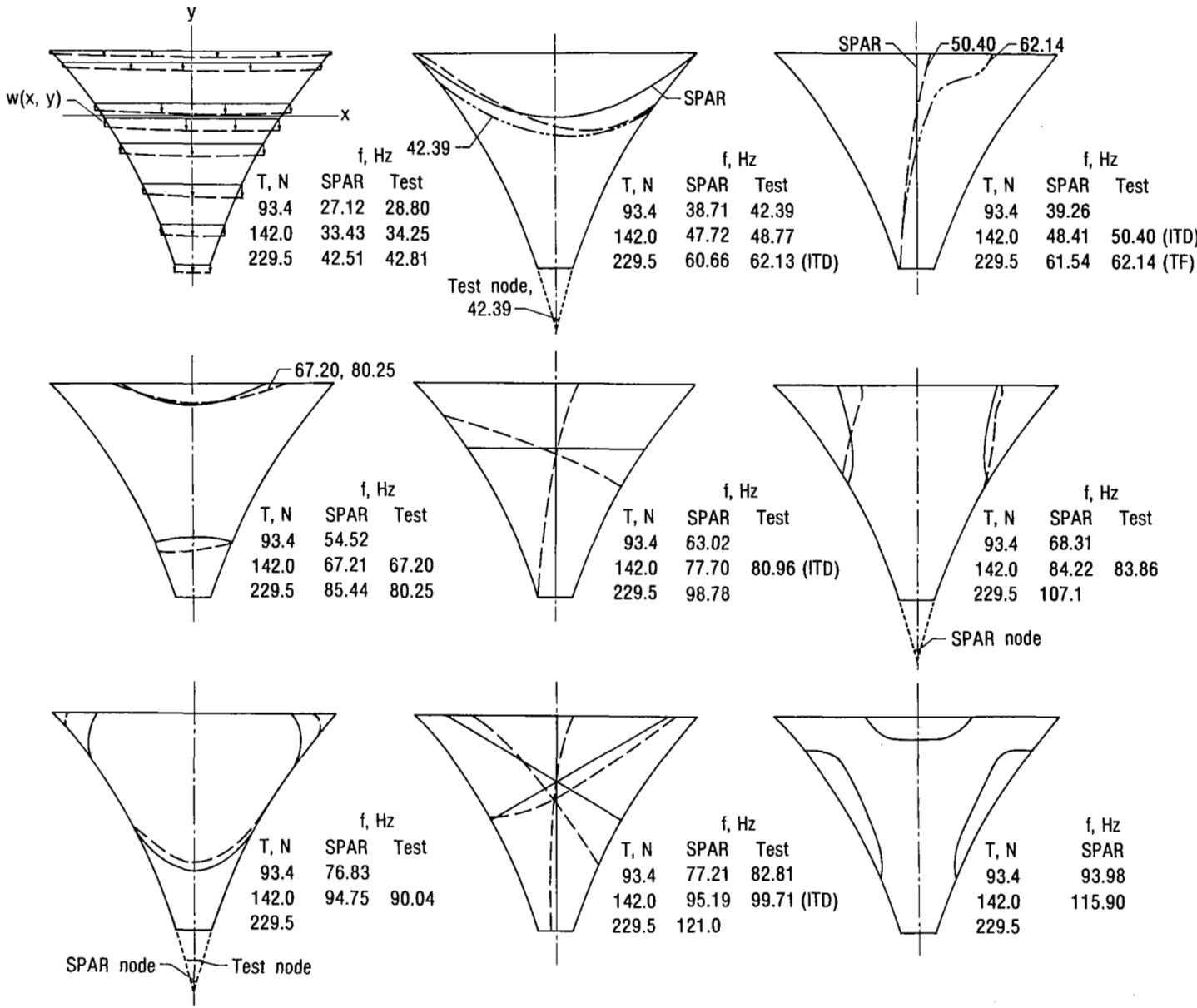

Figure 16.- Membrane experimental and analytical vibration modes in near vacuum of 0.008 to 0.018 atm under equal apex tension loads. All data obtained by sinusoidal input unless otherwise specified.

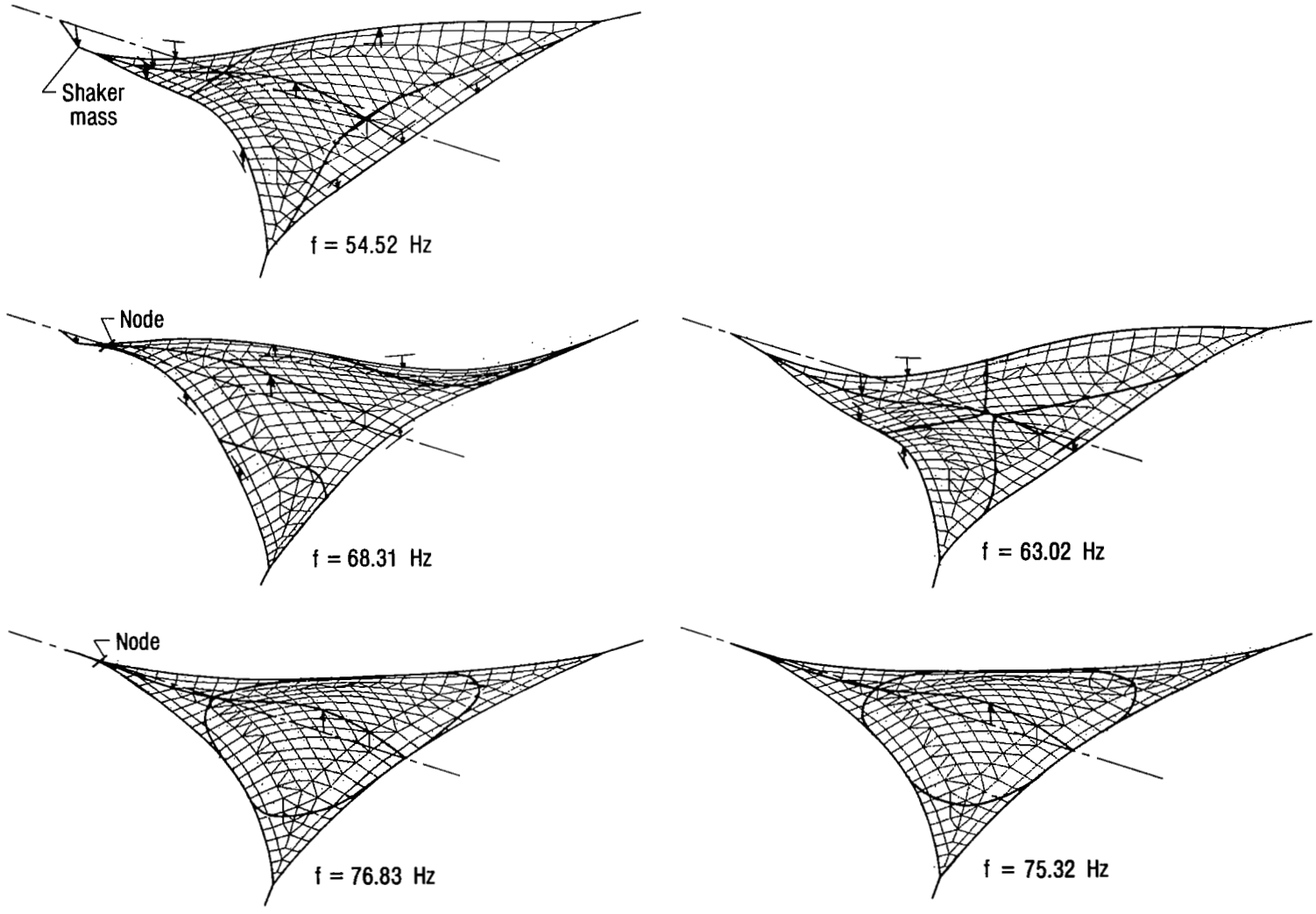

(a) With simulated shaker mass.

(b) Without shaker mass.

Figure 17.- Sensitivity of particular SPAR vibration modes to simulated moving mass of electrodynamic shaker under 93.4 N (21 lb) apex tension.

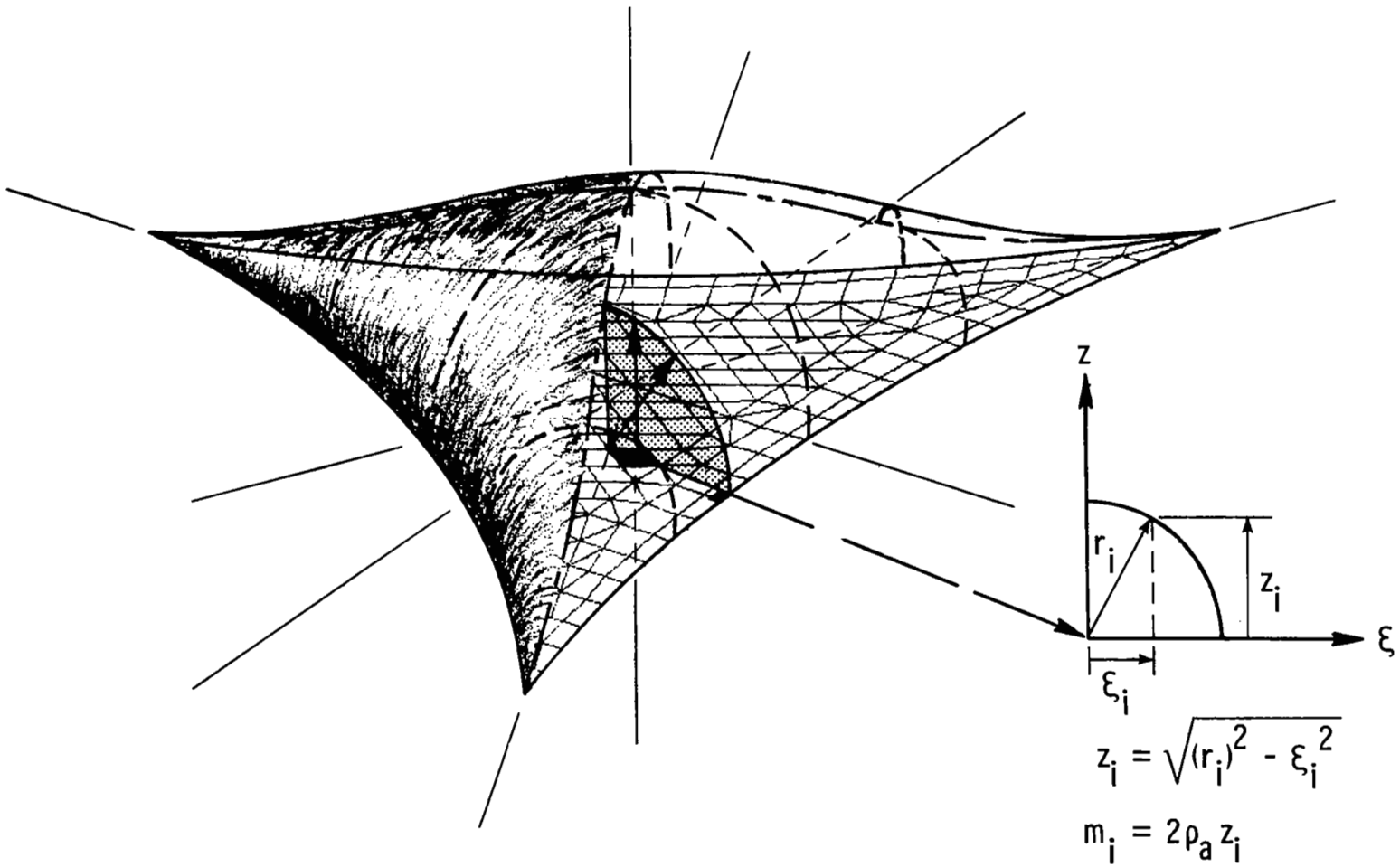

Figure 18.- Ambient-air-mass approximation for three-sided membrane.

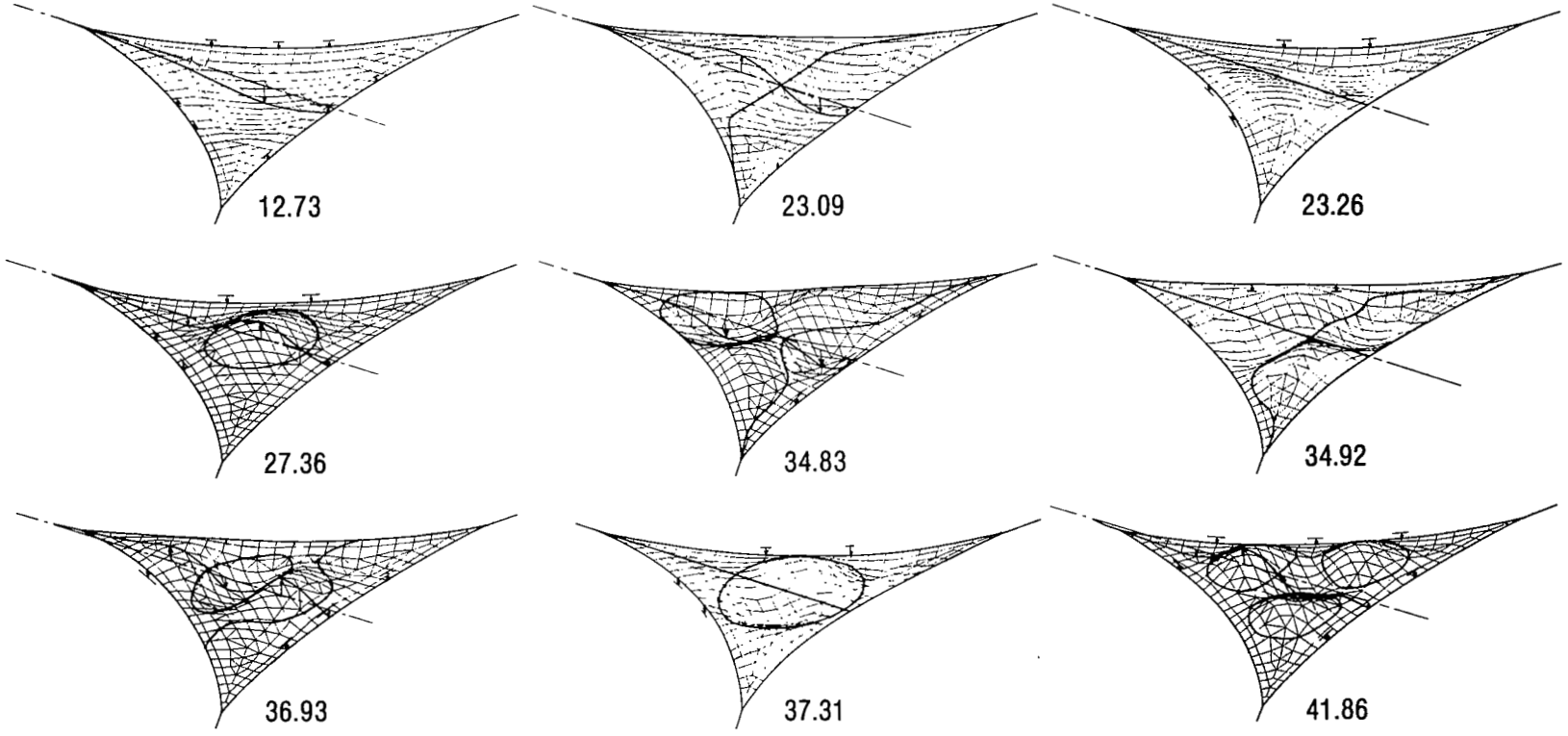

Figure 19.- Analytical vibration mode shapes and frequencies, in hertz, for approximate air mass of 1.0 atm.

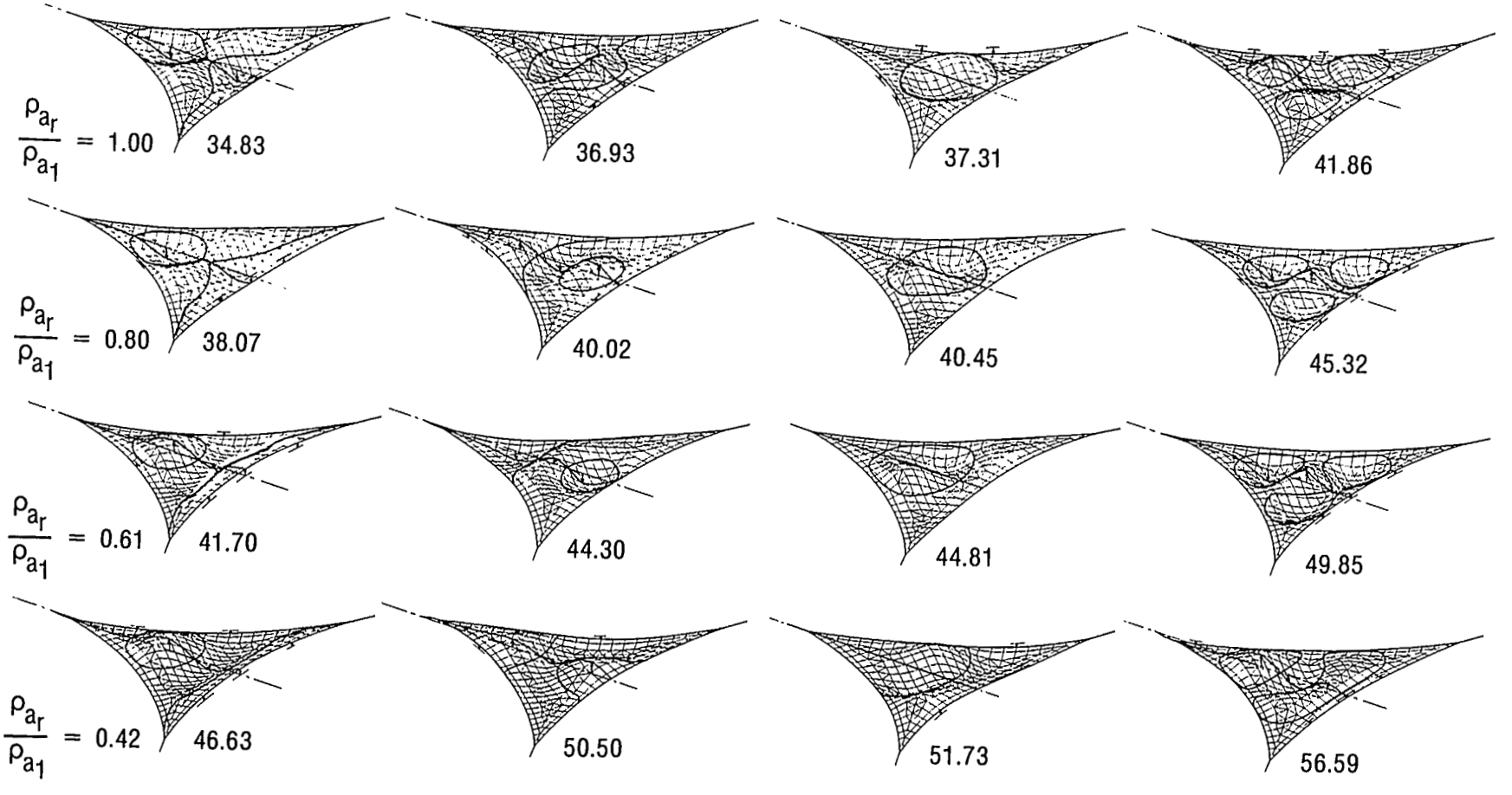

Figure 20.- Analytical vibration mode shapes and frequencies, in hertz, for four air-mass-density ratios. (See also table IV.)

1. Report No.	2. Government Accession No.	3. Recipient's Catalog No.
NASA TP-2095		

4. Title and Subtitle	5. Report Date
VIBRATION STUDIES OF A LIGHTWEIGHT THREE-SIDED MEMBRANE SUITABLE FOR SPACE APPLICATION	January 1983
	6. Performing Organization Code 506-53-43-03
7. Author(s)	8. Performing Organization Report No.
John L. Sewall, Robert Miserentino, and Richard S. Pappa	L-15247
	10. Work Unit No.
9. Performing Organization Name and Address	
NASA Langley Research Center Hampton, VA 23665	11. Contract or Grant No.
	13. Type of Report and Period Covered
12. Sponsoring Agency Name and Address	Technical Paper
National Aeronautics and Space Administration Washington, DC 20546	14. Sponsoring Agency Code

15. Supplementary Notes

16. Abstract

Vibration studies carried out in a vacuum chamber are reported for a three-sided membrane with inwardly curved edges. Uniform tension was transmitted by thin steel cables encased in the edges. Variation of ambient air pressure from atmospheric to near vacuum resulted in increased response frequencies and amplitudes. The first few vibration modes measured in a near vacuum are shown to be predictable by a finite-element structural analysis over a range of applied tension loads. The complicated vibration mode behavior observed during tests at various air pressures is studied analytically with a nonstructural effective air-mass approximation.

17. Key Words (Suggested by Author(s))	18. Distribution Statement
Structural dynamics Antennas Vibrations Large space structures	Unclassified - Unlimited Subject Category 39

19. Security Classif. (of this report)	20. Security Classif. (of this page)	21. No. of Pages	22. Price
Unclassified	Unclassified	48	A03

For sale by the National Technical Information Service, Springfield, Virginia 22161

NASA-Langley, 1983

3 1 1U,D, 830105 S00903DS
DEPT OF THE AIR FORCE
AF WEAPONS LABORATORY
ATTN: TECHNICAL LIBRARY (SUL)
KIRTLAND AFB NM 87117

S